Towards the Large-Eddy Simulation of Complex Engineering Flows with Unstructured Grids

Simone Camarri, Maria Vittoria Salvetti

INRIA

INSTITUT NATIONAL DE RECHERCHE EN INFORMATIQUE ET EN AUTOMATIQUE

Towards the Large-Eddy simulation of complex engineering flows with unstructured grids

Simone Camarri — Maria Vittoria Salvetti

N° 3844

Décembre 1999

THÈME 4

ISSN 0249-6399 ISRN INRIA/RR--3844--FR+ENG

INRIA
SOPHIA ANTIPOLIS

Towards the Large-Eddy simulation of complex engineering flows with unstructured grids

Simone Camarri*, Maria Vittoria Salvetti †

Thème 4 — Simulation et optimisation
de systèmes complexes
Projet SINUS

Rapport de recherche n° 3844 — Décembre 1999 — 48 pages

Abstract: The present work describes the introduction of a large-eddy approach (LES) into an existing code developed for the simulation of aeroelastic problems. The code permits the simulation of compressible flows and employs unstructured grids for the treatment of complex geometry, typical of industrial applications. A RANS approach with a $k-\epsilon$ model was previously used in the code for the simulation of turbulent flows. The subgrid scale model, proposed by Smagorinsky for the closure of the equations in the LES approach, is presented here in the formulation for compressible flows and for unstructured grids. The main issue is to investigate the capabilities of LES combined with a diffusive numerical upwind technology, and the use of a wall-law within this approach. The simulation of the flow around a square cylinder and the analysis of the result sensitivity to different simulation parameters have been used for a first evaluation of the LES model implemented in the code.

Key-words: turbulence modelling - large-eddy simulation - Smagorinsky model - unstructured grids - upwind schemes - wall laws

* INRIA
† Dipartimento di Ingegneria Aerospaziale - University of Pisa

Unité de recherche INRIA Sophia Antipolis
2004, route des Lucioles, B.P. 93, 06902 Sophia Antipolis Cedex (France)
Téléphone : 04 92 38 77 77 - International : +33 4 92 38 77 77 — Fax : 04 92 38 77 65 - International : +33 4 92 38 77 65

Vers la simulation des grandes échelles d'écoulements industriels complexes avec des maillages non structurés

Résumé : On décrit dans ce rapport l'introduction d'une approche de simulation des grandes échelles (LES) dans un logiciel developpé pour la simulation de problèmes d'aèroelasticitè. Ce logiciel permet la simulation d'écoulements compressibles; des maillages non structurés sont employés pour le traitement des géométries complexes, typiques des applications industrielles. Une approche RANS ("Reynolds-averaged Navier Stokes") et un modèle de turbulence de type $k-\epsilon$ étaient précédemment employés pour la simulation d'écoulements turbulents. On présente ici la formulation pour écoulements compressibles et maillages non structurés du modèle de sous-maille proposé par Smagorinsky pour la fermeture des équations dans l'approche LES. Le but principal de ce travail est l'étude du comportement de la simulation des grandes échelles pour des schémas diffusifs de type décentré. On se propose également d'évaluer la possibilité d'utiliser des lois de paroi dans une approche LES. La simulation de l'écoulement autour d'un cylindre carré et l'analyse de la sensibilité des résultats aux différents paramètres sont utilisées ici pour une première évaluation de l'approche LES implémentée.

Mots-clés : modélisation de la turbulence - simulation des grandes échelles - modèle de Smagorinsky - maillages non structurés - schémas décentrés - lois de paroi

Contents

1 Introduction

The direct numerical simulation (DNS) of turbulent flows at high Reynolds numbers, characteristic of engineering applications, is impossible, due to the wide range, in space and time, between the largest and the smallest scales typical of turbulent fluctuations. Moreover, turbulent flows are always three-dimensional and unsteady, and these aspects represent additional problems in the numerical simulation. For this reason, DNS is used only in research applications for the simulation of flows at low Reynolds numbers (typically not higher than 10^3).

The RANS approach to turbulence (Reynolds Averaged Navier-Stokes Equations) is the most widely used in engineering applications at the moment. It consists in filtering the Navier-Stokes equations in time in order to get rid of the high-frequency fluctuations of the flow. As a result, only the mean flow is simulated. The effect of the fluctuations on the time-averaged field is then introduced by modeling. With this approach, larger time steps and coarser grids than in DNS can be used and, hence, the computational costs are reduced. Moreover, the mean flow can be steady and two-dimensional in many cases, and this further reduces the complexity of the problem. However, in this way all information is lost on the turbulent fluctuations, that are entirely given by the model. However, although many closure methods have been proposed for RANS equations, none of them has a general validity.

Another approach to turbulence consists in getting rid of the high-frequency components of turbulence in space and this is the main idea of the large-eddy simulation (LES) approach. Indeed, in LES the Navier-Stokes equations are filtered in space and only the scales larger than the filter width are directly simulated. Thus, the large scales of motion, that are the most interesting for engineering applications, since they are responsible of most of momentum and energy transport, are directly resolved. On the other hand, the effect of the eliminated small scales on the large ones has to be modeled. However, the smaller are the scales of turbulence the more independent they are from the particular considered flow. Therefore, the formulation of closure models of general validity seems to be easier than in RANS. Moreover, within the LES approach we are able to directly account for the three-dimensional and unsteady behavior, typical of turbulence. This is an advantage, since we have realistic simulations of turbulent flows, but it leads to computationally more expensive simulations.

The aim of this work is the choice and the implementation of an LES approach in an existing code, designed for aeroelastic simulations of compressible complex flows, which previously employed a $k-\epsilon$ closure model for a RANS treatment of turbulence. This code, named "AERO", is parallel, employs unstructured grids, implicit/explicit time advancing and TVD schemes. Wall-laws are used for the near-wall treatment.

A critical point in LES is the modeling of the subgrid scales (SGS). Smagorinsky developed in 1963 (see Ref. [25]) the first LES closure method for incompressible flows. This model is used in a wide range of applications. Its simplicity allows it to be a good starting point for the implementation of a new LES approach in an existing code. Moreover, since it represents also the kernel of more recent LES models (i.e. the dynamic Smagorinsky model

developed in the 1991 by Germano [12]) a more complex LES approach could be easily implemented in a second time. For these reasons, the SGS model implemented in the AERO code is the simplest extension of Smagorinsky model to compressible flows.

In spite of its positive features and of the promising results given for different type of flows, LES has been rarely applied to the simulation of engineering flows, characterized hence by high Reynolds numbers and complex geometries. Thus, several specific problems have still to be investigated. Some of them have been treated in the present work.

For instance, a space filter is requested in the LES approach and it can be assumed that the space discretization of the equations acts as a filter on the solution. If unstructured grids are employed in order to treat complex geometries, typical of engineering applications, the definition of a characteristic width of the filter as a function of the local size of the mesh is difficult, since the structure of the filter function is unknown. This is not only an academic problem, since the definition of the filter width is necessary in many closure models. Also, note that very few examples of LES on unstructured grids are available in the literature (Refs. [14, 15, 22] for example).

As said previously, most of the engineering problems are characterized by high Reynolds numbers. With high Reynolds numbers we have problems for the near wall treatment, which can easily become computationally too expansive for industrial applications. Thus, an approximate treatment is necessary. In AERO, the Reichardt wall-law [13] is employed in order to overcome this problem. One issue of the present work is to investigate if such a law is still suitable in LES.

Moreover, robust schemes are needed in order to avoid stability problems in the case of high Reynolds numbers. This is generally obtained by the use of dissipative schemes. On the other hand, the numerical viscosity interferes with the SGS viscosity in a complex way and it can have a strong influence on the solutions. In Ref. [11] it has been shown that TVD schemes are not compatible with LES due to this interaction, that needs to be investigated in order to obtain reliable results from the simulations. In the present study, a sensitivity analysis is carried out by varying some parameters which control the numerical dissipation.

Finally, in engineering applications efficient schemes are needed and implicit time advancing is commonly used, as in the AERO code. However, in the classical LES approach no filter is applied in time. If large time steps are used, as those reachable with implicit schemes, this could act as an additional filter in time. Thus, the following question arises: which is the maximum time step allowable to obtain reliable results without providing a closure model also for time fluctuations? This point is investigated here by carrying out a sensitivity analysis to the maximum CFL number used in the simulation.

The flow around a square cylinder at a Reynolds number of 22000 has been simulated for this first set of tests. This flow has been investigated experimentally by Lyn and Rodi [20, 21], and experimental data are available for the time-averaged as well as for the phase-averaged flow. Also experimental results at different Reynolds numbers are available [1, 6, 16]. Many numerical results are also available in the literature, both from LES [23] and RANS [10, 2] simulations. Thus, this test case is particularly well suited for a first evaluation of the implemented LES approach and for the investigation of the aforementioned aspects.

2 Smagorinky's model for compressible turbulent flows

In the LES approach, the Navier-Stokes equations are filtered in space and the subsequent subgrid scale (SGS) terms need to be modeled in order to directly solve only the flow scales that are larger than the filter width. The problem of SGS modelling can be seen as a passage from "micro" to "macro", in which the object of interest is represented by the laws governing the phenomenon at a macroscopic level. The Navier-Stokes equations are already the result of such a passage: the micro corresponds to the molecular motion and the macro to the fluid particle motion. The constitutive equations represent this passage. The fundamental difference between the two cases consists in the separation between the micro and the macro scales; in the continuous model there is a clear separation between both scales; in the SGS modelling, this separation is somewhat arbitrary. Anyway this similitude is very useful to understand the physical meaning of some of the SGS terms. Indeed, each convective SGS term in the filtered equations has an equivalent viscous term in the un-filtered Navier-Stokes equations. The former ones are the result of the SGS fluctuations, and the latter are the result of the fluctuations at molecular scales. The qualitative effects can be assumed to be the same; they are obviously different from a quantitative point of view.

In the present section, a possible extension of the Smagorinsky model (Ref. [25]) for the LES of a compressible flow is described; the model has been proposed by Lesieur and Comte in Ref. [17].

The great limit of this model consists in the definition of two arbitrary constants: C_s, Pr_t. Those constants will be dependent on the kind of problem to be studied. Besides, a general limit of LES approach lies in the fact that the separation between the small and the large scales of turbulence is somewhat arbitrary. Then the method performance will depend on the characteristic dimension Δ of the filter applied to Navier-Stokes equations.

Furthermore, Smagorinsky's model leads to the definition of an eddy viscosity which is always positive. This means that energy backscatter will not be simulated by this model. As a consequence, this model will be too dissipative and this will stabilize the flow. For this reason, there could be some problems in the prediction of the transition point between laminar and turbulent flow within a boundary layer. Besides, the eddy viscosity will not vanish in a completely laminar flow and near a wall. In order to solve the latter problem, a proper wall-law should be employed.

2.1 Navier-Stokes equations

The Navier-Stokes equations are written here for a compressible fluid. The Einstein index repetition rule is used.

$$\frac{\partial \rho}{\partial t} + \frac{\partial (\rho u_i)}{\partial x_i} = 0 \quad , \tag{1}$$

$$\frac{\partial (\rho u_i)}{\partial t} + \frac{\partial (\rho u_i u_j)}{\partial x_j} = -\frac{\partial p}{\partial x_i} + \frac{\partial \sigma_{ij}}{\partial x_j} \quad , \tag{2}$$

$$\frac{\partial (\rho e)}{\partial t} + \frac{\partial (\rho e u_j)}{\partial x_j} = -\frac{\partial (p u_j)}{\partial x_j} + \frac{\partial (u_j \sigma_{ij})}{\partial x_i} - \frac{\partial q_j}{\partial x_j} \quad . \tag{3}$$

Gravity forces on the fluid have been neglected.

Under the assumption of a perfect, Newtonian gas, the constitutive equations of the fluid are:

$$p = \rho R T \quad , \tag{4}$$

$$e = C_v T + \frac{1}{2} \rho u_i u_i \quad , \tag{5}$$

$$\vec{q} = -K \vec{\nabla} T \quad , \tag{6}$$

$$\sigma_{ij} = \lambda \left(\frac{\partial u_k}{\partial x_k} \delta_{ij} \right) + \mu \left(\frac{\partial u_i}{\partial x_j} + \frac{\partial u_j}{\partial x_i} \right) \quad . \tag{7}$$

Under the Stokes hypothesis, we can assume:

$$\lambda = -\frac{2}{3} \mu \quad . \tag{8}$$

This assumption is equivalent to the neglection of the influence of the isotropic part of the symmetric portion of the tensor $\vec{\nabla} \cdot \vec{v}$ on the viscous stresses. This is a good approximation to study problems in which the point of interest consists in the analysis of the pressure forces exerted by the flow on a body. It leads to significant errors if employed to study certain kind of problems, for example, an acoustic isotropic wave propagation at high frequency.

2.2 Filtering functions

A space filtered field can be associated to any field defined in a given space domain $\mathcal{D}$; this can be obtained through the convolution with a filter function $G_\Delta(\vec{x})$, where Δ is the filter width. In this way the fluctuations in the motion of wavelength smaller than Δ will be eliminated.

Thus, the filtered field is defined, for any quantity f (scalar of vectorial), as

$$\overline{f}(\vec{x}, t) = \int_{\mathcal{D}} f(\vec{y}, t)\, G_\Delta(\vec{x} - \vec{y})\, d\vec{y} \quad . \tag{9}$$

In general the field f can be written as

$$f = \overline{f} + f' \quad , \tag{10}$$

where the term f' represents the fluctuations at scales smaller than the filter width.
It is possible to prove that the filtering process described in (9) is a linear operator; moreover it commutes with temporal and spatial derivatives:

$$\overline{\frac{\partial f}{\partial t}} = \frac{\partial \overline{f}}{\partial t} \quad , \tag{11}$$

$$\overline{\frac{\partial f}{\partial x_i}} = \frac{\partial \overline{f}}{\partial x_i} \quad . \tag{12}$$

When filtering the Navier-Stokes equations for a compressible flow, it is useful to introduce the density-weighted filter (or Favre filter [9]). This is defined as

$$\tilde{f} = \frac{\overline{\rho f}}{\overline{\rho}} \quad , \tag{13}$$

where ρ is a general weighting function; in the case of Navier-Stokes equations it is chosen as the density of the gas.

It is generally assumed that the space discretization of the flow domain, carried out in order to numerically solve the Navier-Stokes equations, acts as a filter on the variables of the flow. Indeed, the numerical solution well represents only the variations of the flow variables with characteristic space length larger than a given value, which is a function of the dimension of the grid and of the particular numerical method employed. For anisotropic unstructured grids, this characteristic length varies in the domain. In the LES approach to turbulence, it is supposed that the filter represented by the space discretization of the domain, which is unknown, can be expressed as in Eq. (9). This assumption is somewhat arbitrary, but it is necessary in order to give an algebraic expression to the SGS terms. It is thus important to analyze the main properties of the real filter. The property (11) is still satisfied. For non-homogeneous grids, property (12) is valid within a certain error, that can be estimated as a a function of the local size of the grid; this point has been analyzed by Vasilyev and Lund in Ref. [28].

2.3 Filtering the Navier-Stokes equations

In this section the Navier-Stokes equations and the constitutive equations, already introduced in Sec. 2.1, are filtered in the physical space using a generic filtering function with the properties described in Sec. 2.2.

Continuity equation Thanks to the adoption of the Favre filter, there are no SGS terms to be modeled in the continuity equation. From the analysis of every single term, we have:

$$\overline{\frac{\partial \rho}{\partial t}} = \frac{\partial \overline{\rho}}{\partial t} \quad ,$$
$$\overline{\frac{\partial \rho u_j}{\partial x_j}} = \frac{\partial \overline{\rho} \tilde{u_j}}{\partial x_j} \quad .$$

Thus, the filtered continuity equation can be written as

$$\frac{\partial \overline{\rho}}{\partial t} + \frac{\partial \overline{\rho} \tilde{u_j}}{\partial x_j} = 0 \quad . \tag{14}$$

Momentum equation By filtering the time derivative we obtain

$$\overline{\frac{\partial (\rho u_i)}{\partial t}} = \frac{\partial (\overline{\rho} \tilde{u_i})}{\partial t} \quad .$$

By filtering the convective part of the momentum transport we obtain:

$$\overline{\frac{\partial (\rho u_i u_j)}{\partial x_j}} = \frac{\partial (\overline{\rho} \tilde{u}_i \tilde{u}_j)}{\partial x_j} - \frac{\partial M_{ij}^{(1)}}{\partial x_j} \quad ,$$

in which $M_{ij}^{(1)}$ is the first SGS term encountered. It takes into account the momentum transport of the SGS scales and it can be expressed as

$$M_{ij}^{(1)} = \overline{\rho} \tilde{u}_i \tilde{u_j} - \overline{\rho u_i u_j} \quad . \tag{15}$$

In order to model $M_{ij}^{(1)}$, it is convenient to split it into its isotropic and its deviatoric part:

$$M_{ij}^{(1)} = \underbrace{M_{ij}^{(1)} - \frac{1}{3} M_{kk}^{(1)} \delta_{ij}}_{T_{ij}} + \underbrace{\frac{1}{3} M_{kk}^{(1)} \delta_{ij}}_{D_{ij}} \quad .$$

The deviatoric part is

$$T_{ij} = M_{ij}^{(1)} - \frac{1}{3} M_{kk}^{(1)} \delta_{ij} \quad , \tag{16}$$

and the isotropic part is

$$D_{ij} = \frac{1}{3} M_{kk}^{(1)} \delta_{ij} \quad . \tag{17}$$

The filtering of the pressure gradient term does not produce any new SGS term and it can be written as

$$\overline{\frac{\partial p}{\partial x_i}} = \frac{\partial \overline{p}}{\partial x_i} \quad .$$

The last term to be filtered is the viscous term. For sake of simplicity, a new tensor P_{ij} will be introduced:

$$P_{ij} = -\frac{2}{3} S_{kk} \delta_{ij} + 2 S_{ij} \quad , \tag{18}$$

in which S_{ij} is the strain rate tensor defined as:

$$S_{ij} = \frac{1}{2} \left(\frac{\partial u_i}{\partial x_j} + \frac{\partial u_j}{\partial x_i} \right) \quad . \tag{19}$$

The constitutive equation for the viscous term can be expressed as

$$\sigma_{ij} = \mu P_{ij} \quad .$$

The filtering of the viscous term in the momentum equation leads to the following result:

$$\overline{\sigma_{ij}} = \overline{\mu P_{ij}} = \mu \widetilde{P_{ij}} + M_{ij}^{(2)} \quad .$$

The tensor $M_{ij}^{(2)}$ is another SGS term, and it represents the transport of viscosity due to the SGS scales fluctuation. It can be expressed as

$$M_{ij}^{(2)} = \overline{\mu P_{ij}} - \mu \widetilde{P_{ij}} \quad . \tag{20}$$

This term could be further developed in more SGS terms. This will not be done here because, as it will be shown in the next sections, this term is negligible if compared to $M_{ij}^{(1)}$.

To sum up, by filtering the momentum equation, we have obtained the following result:

$$\frac{\partial \left(\overline{\rho} \tilde{u_i} \right)}{\partial t} + \frac{\partial \left(\overline{\rho} \tilde{u_i} \tilde{u_j} \right)}{\partial x_j} = -\frac{\partial \overline{p}}{\partial x_i} + \frac{\partial}{\partial x_j} \left(\mu \widetilde{P_{ij}} \right) + \frac{\partial M_{ij}^{(1)}}{\partial x_j} + \frac{\partial M_{ij}^{(2)}}{\partial x_j} \quad . \tag{21}$$

Energy equation By filtering the time derivative term we obtain

$$\overline{\frac{\partial \rho e}{\partial t}} = \frac{\partial \overline{\rho} \tilde{e}}{\partial t} \quad .$$

With the introduction of the thermodynamic state equation for a perfect gas, it is possible to write:

$$\overline{\rho} \tilde{e} = \overline{\rho} C_v \tilde{T} + \frac{1}{2} \overline{\rho} \sum_{j=1}^{3} \widetilde{\left(u_j^2 \right)} \quad . \tag{22}$$

The filtered square of a velocity component can also be written as[1]

$$\overline{\rho} \widetilde{(u_i^2)} = \overline{\rho} \widetilde{u_i u_i} = \overline{\rho} \tilde{u}_i^2 - \left(\overline{\rho} \tilde{u}_i^2 - \overline{\rho} \widetilde{u_i u_i} \right) \quad . \tag{23}$$

[1] In this formula index repetition rule does not apply.

Substituting Eq. (23) in Eq. (22) we obtain

$$\overline{\rho}\tilde{e} = C_v\overline{\rho}\widetilde{T} + \frac{1}{2}\overline{\rho}\sum_{j=1}^{3}\left(\tilde{u}_j\right)^2 - \frac{1}{2}D_{ii} \quad , \tag{24}$$

in which D_{ij} is the isotropic part of $M_{ij}^{(1)}$ as defined in Eq. (17), and it needs to be modeled. The filtering of the convective term in the energy equation leads to

$$\overline{u_i\left(\rho e + p\right)} = \tilde{u_i}\left(\overline{\rho}\tilde{e} + \overline{p}\right) - E_i^{(1)} \quad , \tag{25}$$

in which the SGS term $E_i^{(1)}$ can be expressed as

$$E_i^{(1)} = \left[\tilde{u_i}\left(\overline{\rho}\tilde{e} + \overline{p}\right) - \overline{u_i\left(\rho e + p\right)}\right] \quad . \tag{26}$$

This term could be split at least in two parts, but it is left in this form that is more suitable for further modelling. It represents three distinct physical effects:

1. the transport of energy e due to small scales motions;
2. the change of the internal energy due to the SGS compressibility ($p\vec{\nabla}\vec{v}$));
3. the dissipation of energy due to SGS motions in the pressure field ($\vec{v}\cdot\vec{\nabla}p$).

The filtering of the viscous dissipative terms leads to:

$$\frac{\partial\overline{\sigma_{ij}u_j}}{\partial x_i} = \frac{\partial\overline{\left(\mu P_{ij}u_j\right)}}{\partial x_i} = \frac{\partial\left(\mu\widetilde{P_{ij}}\widetilde{u_j}\right)}{\partial x_i} + \frac{\partial E_i^{(2)}}{\partial x_i} \quad , \tag{27}$$

in which the SGS term $E^{(2)}$ can be expressed as

$$E^{(2)} = \overline{\left(\mu P_{ij}u_j\right)} - \left(\mu\widetilde{P_{ij}}\widetilde{u_j}\right) \quad . \tag{28}$$

This term takes into account the dissipative effect due to the SGS scale transport of viscosity. It can be split at least in three parts having different physical meaning. Indeed, working on Eq. (28), we obtain:

$$E_i^{(2)} = \underbrace{\left(M_{ij}^{(2)}\right)\widetilde{u_j}}_{(a)} + \underbrace{\left(\overline{\sigma_{ij}u_j} - \overline{\sigma}_{ij}\overline{u}_j\right)}_{(b)} + \underbrace{\overline{\sigma}_{ij}\left(\overline{u}_j - \widetilde{u_j}\right)}_{(c)} \quad . \tag{29}$$

Terms (a) and (b) represent the dissipation due to viscous effects in SGS fluctuations. Term (c) represents the dissipation due to viscous and compressibility effects coupled together. The last term to be filtered is the heat diffusion. This leads to

$$\overline{\frac{\partial}{\partial x_j}\left(K\frac{\partial T}{\partial x_j}\right)} = \frac{\partial}{\partial x_j}\left(K\frac{\partial\widetilde{T}}{\partial x_j}\right) + \frac{\partial E_j^{(3)}}{\partial x_j} \quad . \tag{30}$$

The SGS term $E^{(3)}$ can then be expressed as

$$E^{(3)} = \overline{\left(K\frac{\partial T}{\partial x_j}\right)} - \left(K\frac{\partial \widetilde{T}}{\partial x_j}\right) \quad . \tag{31}$$

This term takes into account the heat transfer caused by the motion of the neglected SGS scales.

To sum up, the filtered energy equation can be written as follows:

$$\frac{\partial(\overline{\rho}\widetilde{e})}{\partial t} + \frac{\partial[(\overline{\rho}\widetilde{e}+\overline{p})\widetilde{u}_j]}{\partial x_j} = \frac{\partial(\widetilde{u}_j\widetilde{\sigma}_{ij})}{\partial x_i} - \frac{\partial \widetilde{q}_j}{\partial x_j} + \\ + \frac{\partial}{\partial x_j}\left(E_j^{(1)} + E_j^{(2)} + E_j^{(3)}\right) \quad , \tag{32}$$

in which the SGS terms $E^{(i)}$ are defined in Eq. (26), (28), (31).

2.4 Modelling the SGS terms

The SGS model that is developed in the following section is intended to be used to study flows at high Reynolds numbers (of the order of the problems in engineering applications), at such Mach numbers that low compressibility effects are present in the SGS fluctuations. Besides, this model is not suitable to study flows with high heat transfer and high temperature gradients.

Modelling the SGS terms in the momentum equation The filtering of the momentum equation, already described in Sec. 2.3, led to the definition of three SGS terms: T_{ij}, D_{ij}, $M_{ij}^{(2)}$. Those terms need to be modeled, in order to close the filtered Navier-Stokes equations. The term T_{ij} represents the deviatoric part of the momentum transport tensor $M_{ij}^{(1)}$, defined in Eq. (15). Its analog term, in the un-filtered Navier-Stokes equations, is represented by the tensor σ_{ij}, obtained under the Stokes hypothesis. Since the trace of the tensor T_{ij} is zero (the same is valid for the tensor σ_{ij}), it represents a term that can be added to the viscous terms σ_{ij}. This means that it could be modeled by the definition of an eddy viscosity μ_t, in accordance to Smagorinsky's model extended to compressible flows. As suggested by Lesieur and Comte in Ref. [17], it is possible to write:

$$T_{ij} = \mu_t \widetilde{P_{ij}} \quad , \tag{33}$$

in which the eddy viscosity μ_t can be defined in accordance to the Smagorinsky model [25]:

$$\mu_t = \overline{\rho}\,(C_s\Delta)^2 \left|\widetilde{S}\right| \quad , \tag{34}$$

$$\left|\widetilde{S}\right| = \sqrt{2\widetilde{S_{ij}}\widetilde{S_{ij}}} \quad . \tag{35}$$

The term $M_{ij}^{(2)}$ takes into account the transport of the viscous terms due to small scales fluctuations. However, since the Reynolds numbers are high, this term is negligible if compared to the transport of momentum. Thus it will be neglected.

The last term to be modeled is D_{ij}; it represents the isotropic part of the momentum transport tensor $M_{ij}^{(1)}$; it can be directly added to the thermodynamic pressure. The analogous term in the un-filtered Navier-Stokes equations, due to molecular fluctuation, has been neglected with the assumption (8):

$$\lambda = -\frac{2}{3}\mu \quad .$$

Indeed, due to this assumption, the influence of the isotropic part of the symmetric portion of the tensor $\vec{\nabla}\vec{v}$ has been neglected in the constitutive equations. Thus:

$$tr(\sigma) = 0 \quad .$$

This means that the influence of the momentum transport of molecules, moving in the same direction of a velocity gradient, is negligible if compared to the thermodynamic pressure. In the case of SGS modelling, this effect is not always negligible. It depends on the velocity of the SGS fluctuations. According to Erlebacher *et al.* [7], the term D_{ii} could also be written as

$$D_{ii} = \gamma M_{sgs} \overline{p} \quad , \tag{36}$$

in which M_{sgs} is the SGS Mach number and γ is the specifip heat ratio of the gas. Since the problem class to be studied shows only light compressibility effects, this term is reasonably negligible. Anyway, there are two options for the treatment of this term:

1. to simply neglect it under the following assumption:

$$M_{sgs} \ll 1 \quad . \tag{37}$$

   It is reasonable to assume that M_{sgs} is low when M_∞ is not high, as in the case of the problem class at issue;

2. to model it, as proposed by Yoshizawa [30], in a way which is consistent with the model employed for T_{ij}.

In this section, the first option will be chosen, relaxing the required assumption on M_∞, as suggested by Lesieur and Comte in Ref. [17]. Indeed, the effects of the SGS term D_{ij} can be added to the thermodynamic pressure, leading thus to the definition of a "macro-pressure" Π:

$$\Pi = \overline{p} - \frac{1}{3} D_{ii} \quad . \tag{38}$$

From the analysis of the Eq. (22), it is possible to define a "macro-temperature", using again the term D_{ij}:

$$\overline{\rho}\tilde{e} = \overline{\rho}C_v\left(\widetilde{T} - \frac{1}{2C_v\overline{\rho}}D_{ii}\right) + \frac{1}{2}\overline{\rho}\left(\tilde{u_1}^2 + \tilde{u_2}^2 + \tilde{u_3}^2\right) \quad . \tag{39}$$

Thus, a "macro-temperature" Θ will be introduced

$$\Theta = \widetilde{T} - \frac{1}{2C_v\overline{\rho}}D_{ii} \quad . \tag{40}$$

The filtered equation of state is:

$$\overline{p} = \overline{\rho}R\widetilde{T} \quad . \tag{41}$$

By substituting Eq. (38) and Eq. (40) in Eq. (41) we obtain:

$$\Pi = \overline{\rho}R\Theta + \left(\frac{R}{2C_v} - \frac{1}{3}\right)D_{ii} = \overline{\rho}R\Theta + \left(\frac{3\gamma - 5}{6}D_{ii}\right) \quad . \tag{42}$$

Thus, for mono-atomic gases (for which $\gamma \approx \frac{5}{3}$), the contribution of D_{ii} to Eq. (42) is negligible, independently of the Mach number. In general cases, it is possible to neglect the term D_{ii} under the assumption that the following condition is verified everywhere in the flow field:

$$\left[\frac{(3\gamma - 5)}{6}\right]\gamma M_{sgs}^2 \ll 1 \quad . \tag{43}$$

This leads to an equation of state for the variables Π and Θ which has the same form of Eq. (41):

$$\Pi = \overline{\rho}R\Theta \quad . \tag{44}$$

The condition (43) is less restrictive than (37) and it leads anyway to the neglection of the term D_{ii}.

Modelling the SGS terms in the energy equation The convective term in the energy equation has been written in the following form:

$$\frac{\partial\left(\overline{\rho}\tilde{e} + \overline{p}\right)\tilde{u_i}}{\partial x_i} \quad .$$

Introducing the "macro-pressure" Π defined in Eq. (38), we have:

$$\frac{\partial\left(\overline{\rho}\tilde{e} + \Pi\right)\tilde{u_i}}{\partial x_i} \quad . \tag{45}$$

This leads to a slightly different SGS term from $E^{(1)}$, defined in Eq. (26). This term can be written as

$$F_i^{(1)} = \tilde{u_i}\,(\overline{\rho}\tilde{e} + \Pi) - \overline{u_i\,(\rho e + p)} \quad . \tag{46}$$

Its physical meaning is explained in more detail in Sec. 2.3. This term can be modeled as suggested in Ref. [17]. Here, the term $F^{(1)}$ is modeled in analogy with Smagorinsky model applied for the SGS term $T_{ij}^{(1)}$ in Eq. (33). $F^{(1)}$ is supposed to be proportional to $\vec{\nabla}\Theta$:

$$F_i^{(1)} = C_p \frac{\mu_t}{Pr_t} \frac{\partial \Theta}{\partial x_i} \quad , \tag{47}$$

in which μ_t is the SGS viscosity defined in Eq. (34), in accordance to the Smagorinsky model, and Pr_t is the SGS Prandtl number.
The SGS Prandtl number can be defined in analogy with the Prandtl number for gases:

$$Pr_t = \frac{\mu_t}{K_t} C_p \quad , \tag{48}$$

in which K_t is the SGS conductivity coefficient. To go further in this analogy Pr_t is assumed to be constant.

The SGS term $E^{(2)}$ defined in Eq. (28), which takes into account the dissipative effects due to the SGS transport, is negligible if compared to the SGS convective term $F^{(1)}$. In particular, the contribution (b) in Eq. (29) can be neglected for high Reynolds numbers and low Mach numbers; the same can be said for (c), in which viscous and compressibility effects are coupled, and they both are small in the problem class at issue. The term (a) can also be neglected under the same assumptions. However, the neglection of this contribution is a stronger assumption than the neglection of $M_{ij}^{(2)}$, already done in the modelling of the SGS terms of the momentum equation.

The last SGS term to be modeled in the filtered energy equation is $E^{(3)}$, defined in Eq. (31). It should be slightly modified to introduce the "macro-temperature"; anyway, this term is negligible under the assumption that temperature gradients are weak in the flow, as suggested in Ref. [29] and Ref. [17]. Indeed, this term represents the heat transfer caused by SGS scale fluctuations.

2.5 Resulting LES model for compressible turbulence

The filtered and modeled Navier-Stokes equations are finally the following:

$$\frac{\partial \overline{\rho}}{\partial t} + \frac{\partial \overline{\rho}\tilde{u}_j}{\partial x_j} = 0 \quad , \tag{49}$$

$$\frac{\partial \left(\overline{\rho}\tilde{u}_i\right)}{\partial t} + \frac{\partial \left(\overline{\rho}\tilde{u}_i\tilde{u}_j\right)}{\partial x_j} = -\frac{\partial \Pi}{\partial x_i} + \frac{\partial \left[\left(\mu+\mu_t\right)\left(2\widetilde{S_{ij}} - \frac{2}{3}\widetilde{S_{ii}}\delta_{ij}\right)\right]}{\partial x_j} \quad , \tag{50}$$

$$\frac{\partial(\overline{\rho}\tilde{e})}{\partial t} + \frac{\partial[(\overline{\rho}\tilde{e}+\Pi)\tilde{u}_j]}{\partial x_j} = \frac{\partial \left[\tilde{u}_j\mu\left(2\widetilde{S_{ij}} - \frac{2}{3}\widetilde{S_{ii}}\delta_{ij}\right)\right]}{\partial x_i} + \\ + \frac{\partial}{\partial x_j}\left[\left(\frac{C_p\mu_t}{Pr_t} + K\right)\frac{\partial \Theta}{\partial x_j}\right] \quad . \tag{51}$$

The constitutive equations write:

$$\Pi = \overline{\rho} R \Theta \quad , \tag{52}$$

$$\tilde{e} = C_v\Theta + \frac{1}{2}\left(\widetilde{u}_1^2 + \widetilde{u}_2^2 + \widetilde{u}_3^2\right) \quad , \tag{53}$$

$$\begin{cases} \mu_t = \overline{\rho}\left(C_s\Delta\right)^2\left|\widetilde{S}\right| \quad , \\ \left|\widetilde{S}\right| = \sqrt{2\widetilde{S}_{ij}\,\widetilde{S}_{ij}} \quad . \end{cases} \tag{54}$$

The model described in this section is the simplest extension of Smagorinsky's model to a compressible case. Indeed, Smagorinsky's model is applied for the momentum equations and there is only one SGS term in the energy equations; its structure is very simple, since it derives from the assumption of a constant turbulent Prandtl number for the flow.

The assumptions made on the flow, in order to model the SGS terms of the filtered Navier-Stokes equations, are:

1. high Reynolds numbers, of the order of those typical of engineering applications;
2. low SGS Mach number, so that compressibility effects in the SGS fluctuation are weak;
3. no heat sources or sinks in the flow, which could generate high temperature gradients.

In order to solve the set of equations by a numerical method three aspects need to be treated:

1. the choice of an appropriate value for the two constants C_s and Pr_t; in general they depend on the kind of flow to be simulated. There are many suggestions in literature;
2. the definition, for each discretization element, of the value Δ as a function of its dimensions;
3. a proper understanding of the kind of filtering function represented by the numerical method employed for the solution of the equations.

2.6 Smagorinsky constant for different classes of flows

Many cases of LES simulations of flows by means of the Smagorinsky model are described in literature. The same values for the Smagorinsky constant are usually employed for the same kind of flows. In this section, we will report a brief list of the values usually adopted for C_s and described in Ref. [18].

Lilly [19], working on grids made of cubic elements of side length h and treating the case of incompressible flows, has derived the following result:

$$\Delta_{eq} = h \tag{55}$$

$$C_s = \frac{1}{\pi}\left(\frac{3}{2}C_k\right)^{-\frac{3}{4}} \quad , \tag{56}$$

where Δ_{eq} is the equivalent filter width and C_k is the Kolmogorov constant. Setting the Kolmogorov constant equal to 1.4, value obtained by measurements in the atmosphere (Champagne *et al.* [3]), Eq. (56) leads to the following result:

$$C_s \simeq 0.18 \quad . \tag{57}$$

The main assumptions in order to derive this result are the following:

1. the ensemble-averaged subgrid kinetic-energy dissipation is identical to the dissipation rate ϵ in the Kolmogorov formula:

$$E(k) = C_k \epsilon^{\frac{2}{3}} k^{-\frac{5}{3}} \quad , \tag{58}$$

2. filter function represented by the grid is assumed to be a sharp cut-off filter in Fourier space;

Friedrich and coworkers used a value $C_s = 0.1$ to simulate a back-step flow (Arnal & Friedrich, 1992) and for turbulent pipe flow (Unger & Friedrich, 1994). In the latter case, it is adopted a method suggested by Nikuradse (1933) to simulate the flow near the wall:

$$C_s \Delta x = min\left(l_m, C_s \Delta x\right) \quad ,$$

in which l_m is the mixing length at the wall. However, the authors were not able to correctly simulate the energy transfer mechanism at the wall. $C_s = 0.1$ represents a reduction of the turbulent stresses more than 300% if compared with the value found by Lilly by the method described above.

The value $C_s = 0.2$ has been successfully employed by Deardorff (1971) to simulate isotropic turbulence.

The value $C_s = 0.18$ leads to good results in the simulation of free-shear flows and channel flows; in the latter case, a wall-law is necessary to take into account the boundary layer effect.

2.7 Reichardt wall-law and LES

The Reichardt wall-law is used in AERO in order to avoid the solution of the boundary layer, which represents a problem for high Reynolds flows. Moreover, it guarantees a correct asymptotic behavior at the wall, that represents a problem for the Smagorinsky model.

Indeed, approximate boundary conditions are assigned near the solid boundaries. In particular, a slip condition is imposed on the velocity. The wall-law is used in order to derive the shear stresses caused by the presence of the wall. It can be assumed that the flow is well represented by the numerical solution up to a given distance δ from the wall, depending on the local mesh refinement and on the Reynolds number. This value needs to be assigned as a parameter of the simulation. The Reichardt wall-law can be written as follows (see Ref. [13]):

$$\left(\vec{v}\cdot\vec{t}\right) = U_\tau \left[2.5\ ln\left(1+k\delta^+\right) + 7.8\left(1 - e^{-\frac{\delta^+}{11}} - \frac{\delta^+}{11}e^{-0.33\delta^+}\right)\right] \quad , \tag{59}$$

where $\vec{t}$ is the normalized vector tangent to the wall boundary at a given point, $\delta^+ = \dfrac{\rho U_\tau}{\mu}\delta$ is the non-dimensional value of δ and k is the Von Karman's constant. Once the value of δ is assigned, the non-linear equation (59) can be solved for U_τ. The shear stress at the wall can be derived as follows:

$$\tau_p = \rho U_\tau^2 \tag{60}$$

The coupling of LES with the Reichardt wall-law is not straightforward. Indeed, this wall-law gives an approximate description of the near-wall velocity field that is averaged in time in an interval which is much longer than the turbulent fluctuation characteristic time. Thus, it can be applied together with the RANS approach, which is based on the same assumption. On the contrary, the velocity field of an LES simulation is an instantaneous field, and it describes all the turbulent fluctuations with a spatial characteristic length larger than the width of the space filter. Thus, it is conceptually not clear whether the LES can be coupled directly with the Reichardt wall-law. For the moment this has been done in AERO and the behavior of the wall-law in this case need to be investigated. At the same time we are developing other approaches for the use of this wall-law within the LES.

3 Development of an LES approach to turbulence in the "AERO" code

3.1 AERO code

The AERO code is a Navier-Stokes equations solver for the case of viscous, newtonian, compressible and three-dimensional flows. It is a parallel code and it has been designed for aeroelastic simulations. It employs unstructured grids for description of complex geometries. A mixed finite-volume/finite-element method is used for the space discretization. The finite-volume formulation is used for the convective term and the finite-element one for the diffusive terms of the equations. A $\gamma - \beta$ scheme is used for the convective fluxes [4]. The Roe scheme represents the basic upwind component, and two extra parameters are added:

1. β; it is the upwinding parameter of the MUSCL reconstruction technique; it directly controls the precision (which is of order 3 for $\beta = \frac{1}{3}$) and it has an influence on the dispersion of the scheme;

2. γ_{scheme}; it is the upwinding parameter of the scheme and it directly controls the diffusion of the scheme, which is proportional to the product $(\beta\gamma_{scheme})$.

The amount of numerical viscosity introduced by this scheme plays a crucial role for the success of an LES simulation. For a better understanding of this important point, we will briefly the treatment of the convective fluxes in AERO.

The convective fluxes term can be split into internal fluxes, between a cell and its neighboring ones, and in external fluxes, between the cell and the boundaries of the computational domain:

$$\int_{\partial C_i} \mathcal{F}(W, \vec{n})\ d\sigma = \sum_{j=K(i)} \int_{\partial C_{ij}} \mathcal{F}(W, \vec{n})\ d\sigma + \int_{\partial C_i \cap \Gamma_h} \mathcal{F}(W, \vec{n})\ d\sigma \quad ,$$

in which $K(i)$ is the set of indices of the nodes adjacent to a_i, and ∂C_{ij} (Fig. 1) is defined as:

$$\partial C_{ij} = C_i \cap C_j = [G_{1,ij},\ I_{ij}] \cup [I_{ij},\ G_{2,ij}] \quad .$$

In this section, we will consider only the internal fluxes. They are approximated as follows:

$$\int_{\partial C_{ij}} \mathcal{F}(W, \vec{n})\ d\sigma \simeq \Phi^R(W_i,\ W_j,\ \vec{\nu}_{ij}) \quad , \tag{61}$$

in which

$$\vec{\nu}_{ij} = \int_{\partial C_{ij}} \vec{n} d\sigma \quad . \tag{62}$$

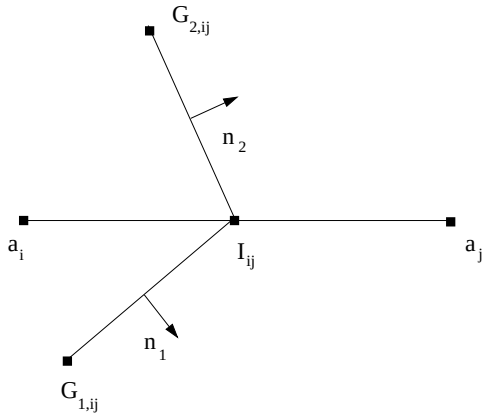

Figure 1: Boundary between two neighboring cells.

Φ^R is an approximated Riemann solver based on the ROE flux function [24]; it is composed by a centered flux term and by an upwind term, proportional to γ_{scheme}, which introduces numerical diffusion and stabilizes the evaluation of the convective fluxes.

$$\Phi^R\left(U,\ V,\ \vec{n}\right) = \frac{\mathcal{F}\left(U,\ \vec{n}\right) + \mathcal{F}\left(V,\ \vec{n}\right)}{2} - \gamma_{scheme} d^R\left(U,\ V,\ \vec{n}\right) \quad , \tag{63}$$

$$d^R\left(U,\ V,\ \vec{n}\right) = \left|\mathcal{R}\left(U,\ V,\ \vec{n}\right)\right| \frac{V-U}{2} \quad . \tag{64}$$

The Roe matrix $\mathcal{R}\left(U,\ V,\ \vec{n}\right)$ is the Jacobian matrix of $\mathcal{F}$ calculated in an average point between U and V:

$$\mathcal{A}\left(W,\ \vec{n}\right) = \frac{\partial \mathcal{F}}{\partial W}\left(W,\ \vec{n}\right) \quad , \tag{65}$$

$$\mathcal{R}\left(W_i,\ W_j,\ \vec{n}\right) = \mathcal{A}\left(\widehat{W},\ \vec{n}\right) \quad . \tag{66}$$

The average point $\widehat{W}$ between W_i and W_j used by Roe is defined as follows [24]:

$$\begin{aligned}
&\widehat{W} = \left(\hat{\rho},\ \hat{\rho}\hat{u},\ \hat{\rho}\hat{v},\ \hat{\rho}\hat{w},\ \hat{e}\right)^T \quad , \\
&\hat{\rho} = \sqrt{\rho_i \rho_j} \\
&\hat{u} = \frac{\sqrt{\rho_i}u_i + \sqrt{\rho_j}u_j}{\sqrt{\rho_i} + \sqrt{\rho_j}} \quad , \\
&\hat{v} = \frac{\sqrt{\rho_i}v_i + \sqrt{\rho_j}v_j}{\sqrt{\rho_i} + \sqrt{\rho_j}} \quad , \\
&\hat{w} = \frac{\sqrt{\rho_i}w_i + \sqrt{\rho_j}w_j}{\sqrt{\rho_i} + \sqrt{\rho_j}} \quad , \\
&\hat{e} = \frac{\sqrt{\rho_i}H_i + \sqrt{\rho_j}H_j}{\sqrt{\rho_i} + \sqrt{\rho_j}} \quad ,
\end{aligned}$$

in which H is the total enthalpy per unit volume:

$$H = \frac{\gamma p}{(\gamma - 1)\,\rho} + \frac{u^2 + v^2 + w^2}{2} \quad .$$

The Jacobian matrix $\mathcal{A}(W,\ \vec{n})$, defined in Eq. (65), can be diagonalised and it has real eigenvalues. Thus, it is possible to split the matrix $\mathcal{A}$ in two parts, one with positive and one with negative eigenvalues:

$$\mathcal{A} = \mathcal{A}^+ + \mathcal{A}^- \quad . \tag{67}$$

The spatial approximation of the convective fluxes, obtained by the Roe function, is first order accurate. MUSCL linear reconstruction method ("Monotone Upwind Schemes for Conservation Laws"), introduced by Van Leer [27], is employed to raise the order of precision of the Roe scheme. The basic idea consists in using reconstructed value of W at the boundary between the two cells as the argument of the Roe function:

$$\int_{\partial C_{ij}} \mathcal{F}(W, \vec{n})\ d\sigma = \Phi^R\left(W_{ij},\ W_{ji},\ \vec{\nu}_{ij}\right) \quad , \tag{68}$$

in which $W_{ij} = [W]^-_{I_{ij}}$ and $W_{ji} = [W]^+_{I_{ij}}$ are values of W at the left and at the right hand side of the point I_{ij} (Fig. 2); they are extrapolated from the values of W in the nodes $a_i,\ a_j$. This extrapolation is performed by a class of numerical methods known as β-schemes:

$$\left\{\begin{array}{l}
W_{ij} = W_i + \frac{1}{2}\left[(1-2\beta)\left(\vec{\nabla}W\right)^C + 2\beta\left(\vec{\nabla}W\right)^D_i\right]\vec{a_i a_j} \quad , \\
\\
W_{ji} = W_j - \frac{1}{2}\left[(1-2\beta)\left(\vec{\nabla}W\right)^C + 2\beta\left(\vec{\nabla}W\right)^D_j\right]\vec{a_i a_j} \quad .
\end{array}\right. \tag{69}$$

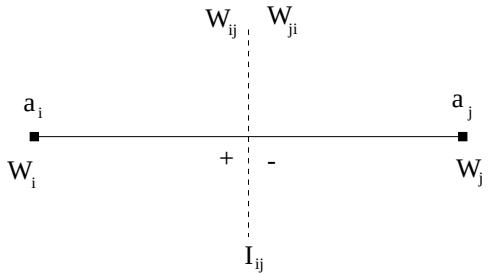

Figure 2: Position of W_{ij}^{-} and W_{ji}^{+}.

The term $\left(\vec{\nabla}W\right)^{C}$ in Eq. (69) is the approximation of the gradient of W, evaluated by a centered numerical scheme in the interval $[a_i,\ a_j]$. The term $\left(\vec{\nabla}W\right)_i^{D}$ is a totally upwind gradient of the vector W, evaluated on the node a_i as follows:

$$\left(\vec{\nabla}W\right)_i^{D} = \frac{\sum\limits_{k=N(i)} \int_{T_k} \vec{\nabla}W}{\sum\limits_{k=N(i)} V\left(T_k\right)} \quad , \tag{70}$$

in which $N(i)$ are the indices of the elements having a_i as a node and $V\left(T_k\right)$ is the measure of the k-th element of the mesh. The same can be told for the other term $\left(\vec{\nabla}W\right)_j^{D}$. For an analysis of the precision of the scheme, we consider a bidimensional advection equation:

$$\begin{cases} \dfrac{\partial U}{\partial t} + \vec{V}\cdot\vec{\nabla}U = 0 \qquad (x,y,t) \in \mathbb{R}^2 \times [0,\ \infty[\quad , \\ \\ U(x,y,0) = U_0(x,y) \quad (x,y) \in \mathbb{R}^2 \quad , \end{cases} \tag{71}$$

$$\vec{V} = (a,\ b)^T \quad . \tag{72}$$

If the $\gamma - \beta$ scheme is employed for the spatial discretization of this problem on a regular grid of the Friedrichs-Keller type, under the assumption that the nodes are equispaced in both directions ($\Delta_x = \Delta_y = h$), the equivalent problem associated to this scheme is the

following one:

$$
\begin{aligned}
(-aU_x - bU_y)_{approx} =& (-aU_x - bU_y) + \left[\frac{a}{6}(3\beta - 1)\, h^2\right] U_{xxx} + \\
& \left[\frac{(3\beta-1)}{6}(a+b)\, h^2\right](U_{xxy} + U_{xyy}) + \left[\frac{b}{6}(3\beta - 1)\, h^2\right] U_{yyy} + \\
& - \left\{\gamma_{scheme}\left[\frac{\beta}{12}\Big(|(a+b)\, h| + |(2a-b)\, h|\Big)\right] h^2\right\} U_{xxxx} + \\
& - \left\{\gamma_{scheme}\left[\frac{\beta}{3}\Big(|(a+b)\, h|\Big)\right]\right\}(U_{xxxy} + U_{xyyy}) + \\
& - \left\{\gamma_{scheme}\left[\frac{\beta}{2}(|(a+b)\, h|)\right] h^2\right\} U_{xxyy} + \\
& - \left\{\gamma_{scheme}\left[\frac{\beta}{12}(|(a+b)\, h| + |(2b-a)\, h|)\right] h^2\right\} U_{yyyy} + O(h^4)
\end{aligned}
$$

The approximated solution that we obtain by the $\gamma - \beta$ scheme for the problem (71) is the exact solution of the equivalent differential equation written above. It is possible to note that, for $\beta = \frac{1}{3}$ the scheme is of order 3 and that, as already told, β influences the diffusion of the scheme and the dissipation is controlled by the product $(\beta\gamma_{scheme})$

An implicit second order accurate scheme is used for the time advancing. Explicit time advancing is also possible with AERO. A RANS approach for turbulence, with a $k-\epsilon$ closure model, is implemented in the code. Reichardt wall-law is used for the approximate near-wall treatment. For a more detailed description of the AERO code, we refer to Ref. [8].

3.2 Definition of the equivalent filter width

Generally, in the cases of LES with Smagorinsky model on unstructured grids an extrapolation of the definitions given for Δ_{eq} in structured grids is employed. In the AERO code, the following definition has been employed for the Smagorinsky model:

$$\Delta_{eq}^{(j)} = max_{i=1,..,6}\left(\Delta_i^{(j)}\right) \quad , \tag{73}$$

in which $\Delta_i^{(j)}$ is the length of the i-th side of the $j-$th element. This definition has been chosen because we think it is representative of the actual spatial resolution of the numerical solutions. At the same time, tests have been made on another definition of Δ_{eq}, already employed in LES with unstructured grids by Marquez [22]:

$$\Delta_{eq}^{(j)} = \sqrt[3]{Vol\,(T_j)} \quad , \tag{74}$$

in which $Vol\,(T_j)$ is the volume of the $j-$th tetrahedron of the mesh. This is the extrapolation of definition derived by Deardorff [5] to the case of unstructured grids.

The two different definitions described above have been tested with a-priori tests and the results are described in Sec. 4.4.

New definitions for the equivalent filter width need to be developed for very heterogeneous meshes, which can be easily encountered in engineering applications. A typical example is a flow with singularities, as it is the case of shock waves. Indeed, the mesh will be much more refined in localized areas near the singularities, but, at the same time, we are not interested in solving all the turbulence scales in those regions. On the other hand, the real resolution at the interface between a refined and a coarser mesh is something in between what we have in the two cases separately. Thus, a realistic definition of the equivalent filter width should take into account not only the single discretization element, but also the shape of the other neighboring elements, especially for heterogeneous meshes.

The testing of new equivalent filter width for unstructured heterogeneous grids is one of the future developments of the present work.

4 Results

4.1 Test case

In this section we report the results obtained in the LES simulation of the flow around a square cylinder at a Reynolds number of 22000. Experimental results for this flow are given by Lyn and Rodi [20, 21] in the incompressible case. The simulations presented here have been performed with a Mach number $M = 0.1$. Numerical results are also available in the literature and, in particular, those obtained by the contributors to a recent workshop, devoted to the large-eddy simulation of the same test case, are documented in Ref. [23].

In this flow, the separation points are fixed by the geometry of the body. The flow separates when it is still laminar, it generates a shear flow just behind the upwind face and, afterward, it becomes unstable and turbulent. On the upper and lower walls there are recirculation regions and there is no a re-attachment of the flow. As a consequence, this test case is particularly useful to check the behavior of the model in the treatment of completely separated and turbulent wakes. Since the transition does not occur near the wall and there are no re-attachment points, this test is not suitable to evaluate the efficiency of the wall-law in describing those phenomena. Moreover, since the Mach number is low, the energy equation plays a secondary role in the solutions and the SGS term in this equation is not completely validated by the present test-case. The turbulent Prandtl number (see Eq. 48) has been assumed equal to $Pr_t = 0.9$ in all the simulations described.

Two different computational domains have been used for the simulations; their dimensions are reported in Tab. 1, with reference to the Fig. 3. The domain (a) was originally built for the $k - \epsilon$ model, that is not able to simulate the three dimensional effects of turbulence. In the large eddy simulations, this domain has been found to be too short to allow a proper description of the characteristic modes of the flow in the direction of the cylinder axis. However, it has been used in order to test the sensitivity of the results to some of the simulation parameters. Indeed, although for this reason a quantitative agreement with the experimental results can not be expected, indications can be obtained on the qualitative effect of the different parameters. For a more detailed comparison with the experiments, the domain (b) has been used, whose dimensions have been chosen in accord to the suggestions given for the LES workshop described in Ref. [23]. The only difference is in the distance of the outflow surface from the cylinder, which is smaller in our case.

At the inflow, the flow is supposed to be undisturbed. At the outflow, Steger-Warming [26] conditions are used. Those boundary conditions are well suited for flows in which the convective terms are dominant on the diffusive terms, as in the case at issue, since the Reynolds number is high. In the y and z directions, slip boundary conditions are imposed. In the simulations in Ref. [23] periodic boundary conditions were used in the z direction to reproduce the flow around an infinite cylinder. The effects of no slip boundary conditions imposed in our LES are discussed in Sec. 4.6. A uniform flow has been assumed as initial condition for the simulations. On the body, the Reichardt wall-law has been used for an approximate near-wall treatment. Almost all of the simulations described in Ref. [23] have also been performed with wall-laws.

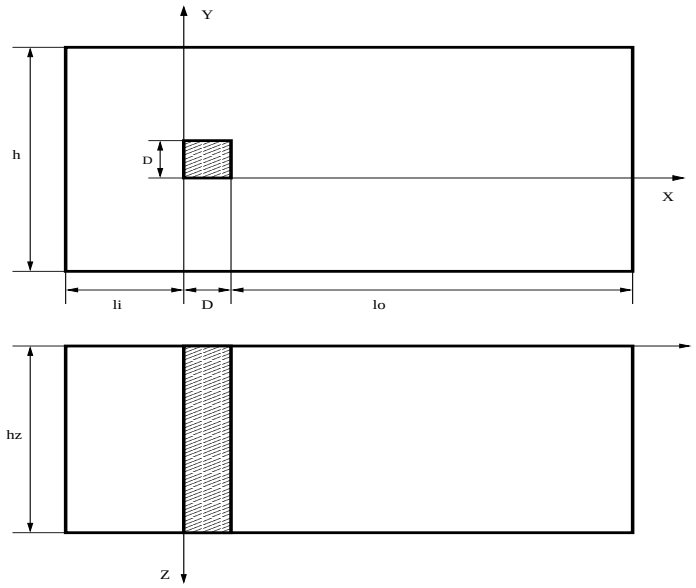

Figure 3: Computational domain.

	l_i/D	l_o/D	h/D	w/D	N. nodes	N. elements
domain (a)	1.5	7	6	0.36	43154	224657
domain (b)	4.5	9.5	14	4	102134	588056

Table 1: Dimensions of the computational domain (see fig. 3).

The Strouhal number and (time averaged) drag coefficient are the global parameters of particular interest for the present flow; they are defined as follows:

$$S_t = \frac{fD}{U_\infty} \quad , \tag{75}$$

$$C_d = \frac{2D_r}{\rho_\infty U_\infty D h_z} \tag{76}$$

in which f is the vortex shedding frequency, D and h_z are respectively the side length and the height of the cylinder (see Fig. 3) and D_r is the drag. The vortex shedding frequency has been estimated from the peak in the lift spectrum.

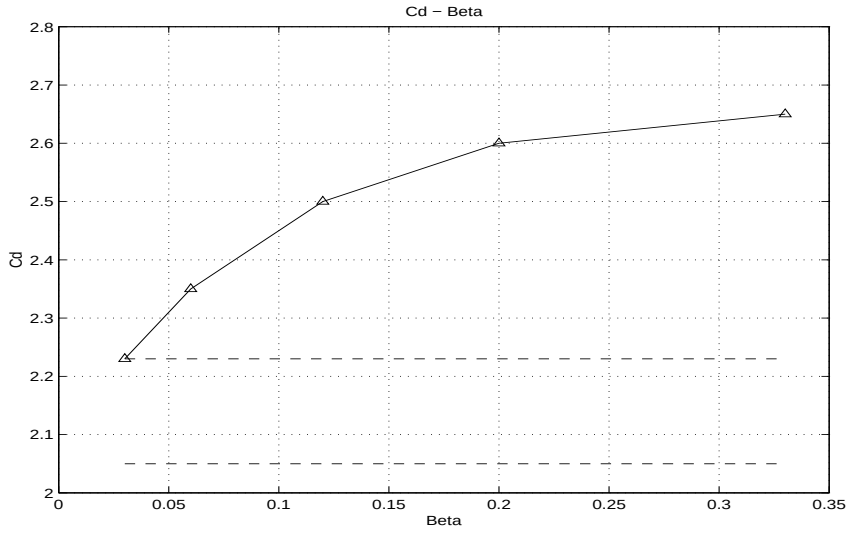

Figure 4: Effect of the upwinding parameter β on the mean drag coefficient.

4.2 Sensitivity to the numerical viscosity

The upwinding parameter β, introduced in Sec. 3.1, controls the degree of upwinding in the evaluation of the gradients for the MUSCL reconstruction method. When we have $\beta \simeq 0.33$, the scheme for the convective fluxes evaluation is third-order accurate for linear systems (i.e. advection equations), as shown in Sec. 3.1; the main part of error is a numerical diffusion term, and it can interfere with the SGS viscosity of the Smagorinsky model. The numerical diffusion term does not produce the same effects on the solution as the SGS viscosity one, since it is proportional to the fourth spatial derivatives of the velocities while the SGS viscosity term is proportional to the second spatial derivatives of the velocities.

In order to test the effect of β on the solution, five simulations have been carried out on the domain (a), with $\beta = 0.03,\ 0.06,\ 0.12,\ 0.2,\ 0.3$. The other scheme parameter, which directly controls the amount of numerical viscosity, is set to $\gamma_{scheme} = 1.0$ in this first set of simulations. The values of the mean drag coefficient and of the Strouhal number obtained in the simulations have been plotted as functions of β in Fig. 4 and in Fig. 5 respectively. The dotted line represents the scatter in the experimental data. As already told, the goal of these tests is not a quantitative comparison with the experimental data but only the qualitative study of the effects of the simulation parameters on the solutions.

While it seems there is not a precise effect on the Strouhal number, the drag coefficient systematically increases when β is increased and the solution tends to be more different from the experimental one. This experience suggests the choice of a low β; on the other

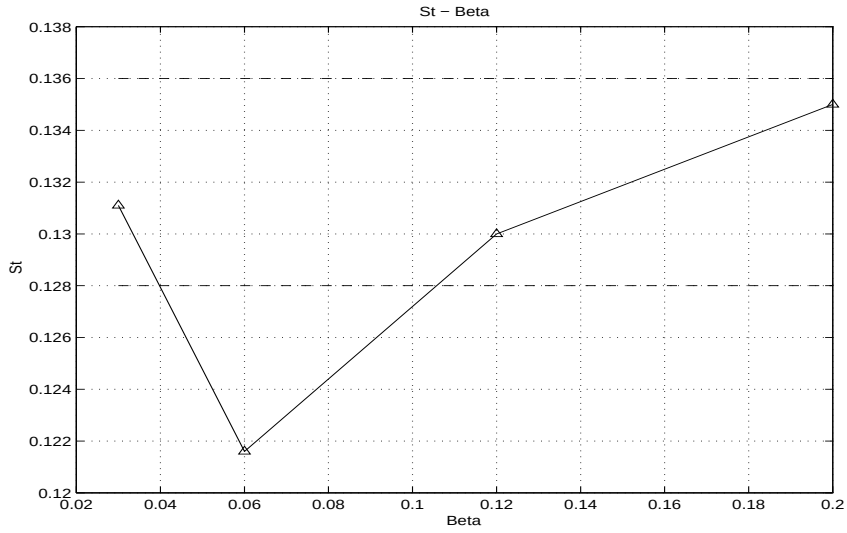

Figure 5: Effect of the upwinding parameter β on the Strouhal number.

hand, this parameter can not be decreased too much, otherwise we risk to have numerical instability in the simulation.

The same behavior of the mean drag coefficient and of the Strouhal number has been observed by varying the parameter γ_{scheme} and keeping $\beta = 1/3$. This is represented in Fig. 6. It is interesting to note that for low values of γ_{scheme} the value of C_d tends to stabilize; this confirms that the amount of numerical viscosity should be maintained as low as possible to reduce spurious effects on the solution.

In the literature there is a general agreement on the fact that the numerical viscosity interferes with the SGS viscosity and that LES simulations should be performed with central schemes or with low upwinding. In particular, in Ref. [11] the compatibility between the shock capturing schemes and the LES is analysed and it is shown that those schemes are not compatible with a SGS model. This is in accord to the results presented here. As a consequence, in order to perform LES simulations with AERO, the shock capturing feature of the TVD scheme employed will not be used. Indeed, the scheme will be altered by tuning the degree of upwinding in order to reach a minimum level of stability for the simulations and, at the same time, to keep the numerical viscosity as low as possible. This is possible for the test-case at issue since we do not have shock-waves in the flow simulated. In the cases where discontinuities are present in the flow, there are two possible alternatives in order to guarantee the stability of the simulation:

1. to use a shock-detecting method and to use the full upwinding of the schemes in localised areas around the discontinuities, as suggested in Ref. [11];

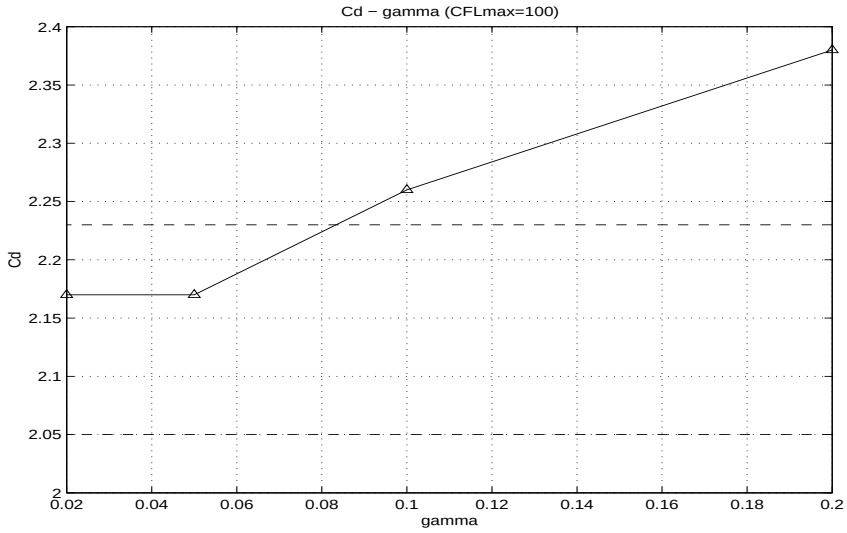

Figure 6: Effect of parameter γ_{scheme} on the mean drag coefficient ($\beta = 0.33$).

2. to refine the mesh where we expect disconinuities for the flow.

The second solution is easier to be applied in cases where at least the tipology of the flow can be guessed and for stationary problems. In the case of instactionary and transonic problems, where the shock-waves moves in time, the solution (2) can be used only moving the mesh in order to follow the shock wave, and this can be very complex.

Some additional simulations have been performed without any SGS viscosity in order to check the influence of the SGS model on the solutions. As expected, the simulations with $\gamma_{scheme} = 1$ converged only for $\beta \geq 0.12$. This is a proof that the SGS viscosity acts as a stabilizing term in the equations, as accepted in literature. At the same time, the results obtained without SGS model were physically not consistent: for instance a well defined vortex shedding frequency was not found. This proved that, at least for this test-case, the numerical viscosity can not replace the SGS viscosity and a turbulence model is thus necessary. This conclusion has been also drawn for different types of flows in previous studies in the literature.

Furthermore, it has been recently shown in the literature [11] that for TVD schemes the numerical error committed in the discretization of the equations could be of the same order of magnitude of the SGS viscosity. In this case, the ratio between the SGS viscosity and the numerical error for the discretization has not been estimated and this point needs to be investigated. Nevertheless, the sensitivity analysis that we carried out indicates that, if the parameters γ_{scheme} and/or β are maintained low enough, the numerical viscosity has

C_s	C_d	S_t
0.1	2.23	0.131
0.17	2.5	0.117

Table 2: Behavior of the mean drag coefficient and of the Strouhal number with variations of the Smagorinsky constant.

plausibly a negligible effect on the solution. We should remark however that in that case the capability of capturing shocks is lost.

4.3 Sensitivity to the Smagorinsky parameter

The Smagorinsky constant is dependent on the kind of flow considered. From an analysis of different LES simulations described in the literature (see for example Ref. [29]), it seems that $C_s = 0.1$ could be an acceptable value for the Smagorinsky constant in the flow at issue. However, the Smagorinsky constant has been varied within the range $C_s \in [0.1, 0.17]$ to test the effect of the SGS viscosity on the solution. It has been observed that, by increasing C_s (thus increasing the SGS viscosity), the mean drag coefficient increases while the Strouhal number decreases. However, the sensitivity of those global variables to a remarkable variation of C_s is rather low. This is probably due to the particular test case at issue. Indeed, as already told, the separation points are fixed by the geometry of the body and the transition phenomena do not change the typology of the flow. As an example, in Table 2 we compare the results of two simulations performed with $C_s = 0.1$ and $C_s = 0.17$ respectively, in terms of the mean drag coefficient and of the Strouhal number. The other input parameters have been set to the following values: $\gamma_{scheme} = 1.0$, $\beta = 0.03$, Δ_{eq} given by Eq. (73). Since the SGS viscosity is proportional to the square value of C_s, assuming $C_s = 0.1$ or $C_s = 0.17$ leads to a difference of a factor 2.89 in the SGS viscosity. The variations of the Strouhal number and of the mean drag coefficient are approximately of 11%.

4.4 Equivalent filter width

In order to understand the differences between the two definitions of the equivalent filter width given in Sec. 3.2, a-priori tests have been performed. An instantaneous velocity field, obtained in a LES simulation, with $C_s = 0.1$, $\gamma_{scheme} = 1.0$, $\beta = 0.03$ and Δ_{eq} given by Eq. 73, has been considered; the ratios between the SGS viscosity (μ_t) and the molecular viscosity (μ) have been evaluated by the two different definitions using the given velocity field. In Fig. 7 we have plotted the ratio $\frac{\mu_t}{\mu}$ for the definition (73) of the filter width.

By overlapping the mesh to the isovalues (Fig. 8), it is possible to note that peaks are concentrated in a few nodes located on the biggest elements far from the body. This is interesting since it gives an idea of the sensitivity of the Smagorinsky model to the mesh size. Indeed, turbulent viscosity is a function of the local size of the mesh due to the definition

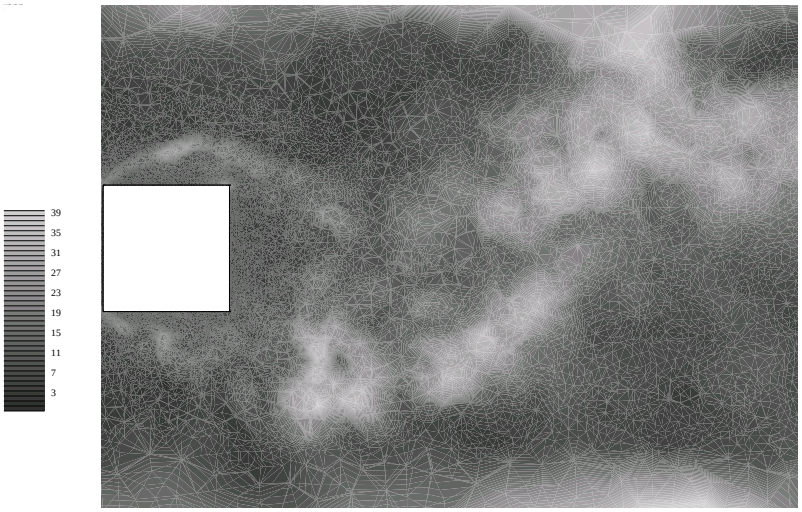

Figure 7: Ratio between the SGS viscosity and the gas viscosity; $C_s = 0.1$, Δ_{eq} defined in Eq. (73).

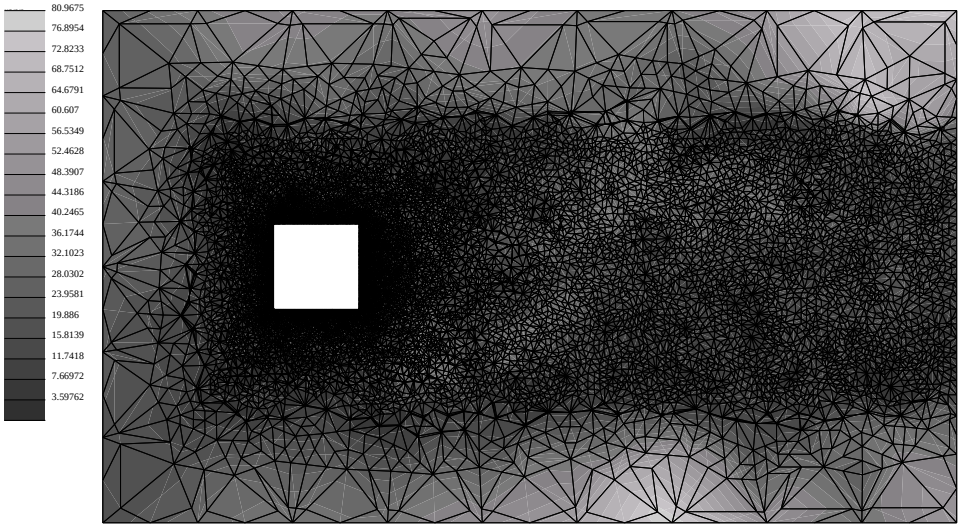

Figure 8: Ratio between the SGS viscosity and the gas viscosity; $C_s = 0.1$, Δ_{eq} defined in Eq. (73).

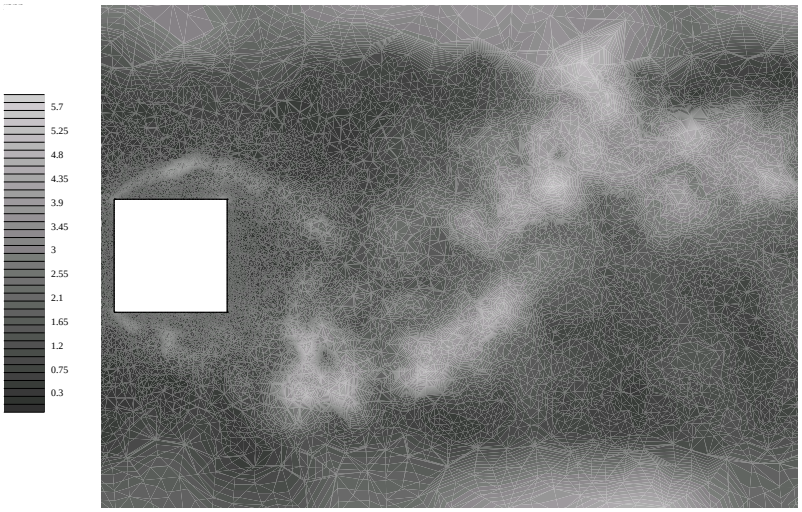

Figure 9: Ratio between the SGS viscosity and the molecular viscosity; $C_s = 0.1$, Δ_{eq} defined in Eq. (74).

of the equivalent filter width. Thus, on bigger elements, even if the velocity gradients are lower, we have however a remarkably large turbulent viscosity. This indicates that abrupt changes in the element size should be avoided and the grid refinements should be as regular as possible with this SGS model. In the wake, where the mesh is refined enough, there are peak values of around 38, as reported in Table 3.

The ratio between the SGS and the molecular viscosity for the definition (74) of Δ_{eq} has been plotted for the same velocity field in Fig. 9. The Smagorinsky constant is still $C_s = 0.1$. As it is possible to see from those figures, the qualitative behavior is the same, but the SGS viscosity obtained with this latter definition is approximately 10 times lower than that obtained with Eq. (73) (see Tab. 3). This difference is much more contained for structured grids with usual aspect ratios for the elements.

In the LES simulations on unstructured grids described in the literature, this second definition of Δ_{eq} is used with a Smagorinsky constant of $C_s = 0.18$ (see Ref. [22]). In this case, the values of the ratio between the SGS and the gas viscosity have again the same qualitative behavior as in Fig. 9, but the values need to be multiplied by a scaling factor of 3.24.

As a conclusion, the two different definitions of the filter width that have been tested here differ only from a quantitative point of view while the distribution of μ_t/μ in the flow field is very similar. As a consequence, they should be equivalent with a proper choice of the Smagorinsky constant. At the same time, it has been shown in Sec. 4.4 that the solutions

	Min.	Mean	Max.	Max. (wake)
$\Delta_{eq}^{(1)},\ C_s = 0.1$	0.2	5.7	85	37
$\Delta_{eq}^{(2)},\ C_s = 0.1$	0.0	0.7	8.5	5.3
$\Delta_{eq}^{(2)},\ C_s = 0.18$	0.11	2.4	27.5	17.2

Table 3: Values of the ratio between SGS and gas viscosity; $\Delta^{(1)}$ and $\Delta^{(2)}$ correspond to the definitions (73) and (74) respectively.

are not sensitive to a remarkable variation of the Smagorinsky constant. Thus, we expect that the two different filters proposed here are almost equivalent at least for this particular flow and, thus, we did not repeat the simulation with the definition (74).

4.5 Time advancing

In the classical LES approach, only a filter in space is applied to the equations, while all the turbulence fluctuations in time are assumed to be resolved. However, industrial codes usually use implicit schemes in order to increase the allowed time-step size and, thus, the speed of the simulations. This is particularly interesting when complex geometries lead to very heterogeneous meshes. It is then probably wrong that the smallest cell size should govern the length of the time step. If the time step used in the simulation is too large, the time discretization could be seen as a filter on the solution and this should be taken into account by an additional closure model. Thus the following question arises: which is the maximum time step allowable without providing any closure model in time?

The minimum filter width Δ_{min} we have in all the grid is representative of the minimum turbulence spatial scale we can resolve in the flow. If we have a reference velocity U_∞, as it is the case of the test case at issue, we can associate a characteristic time τ to this length in the following way:

$$\tau = \frac{\Delta_{min}}{U_\infty} \quad .$$

The time scale τ gives an order of magnitude of the time step we can use in the simulation without the risk of loosing information in time. For the particular test case at issue, this rule of thumb gave positive results. Indeed, the time interval estimated by this procedure corresponds to a CFL number of about 10. We performed several simulations changing, at each time, only the maximum CFL number and using an implicit scheme. The corresponding lift curves are plotted in Fig. 10. The differences between the curves obtained with $CFL = 100$ and $CFL = 50$ are relevant. This means that, with the first value of CFL, we loose important information on the turbulent fluctuation. The same behavior is observed until a $CFL = 10$ is reached. Indeed, the differences between the curves obtained with $CFL = 10$ and $CFL = 5$ are almost coincident.

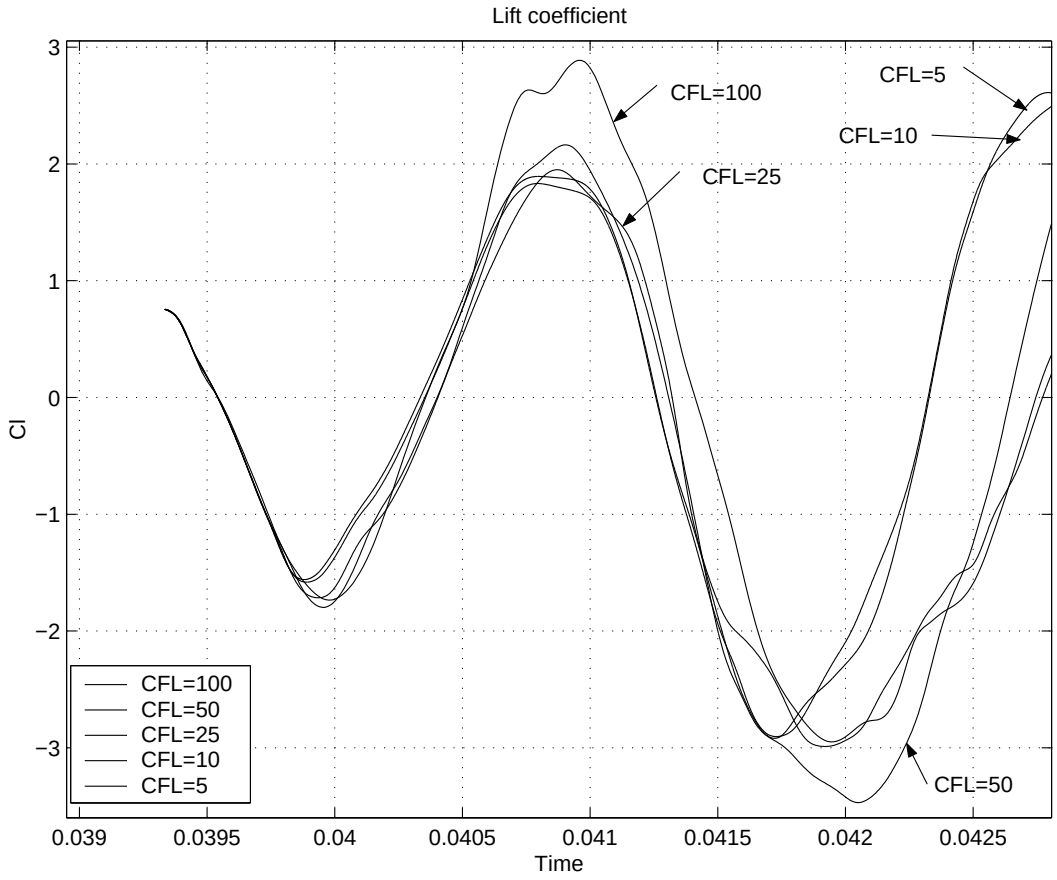

Figure 10: Lift curves obtained with different CFL numbers.

	$\overline{C_l}$	$C_{l,rms}$	$\overline{C_d}$	$C_{d,rms}$	S_t	l_r
Simulation	0.0061	0.3920	1.90	0.058	0.138	1.58
LES results [23]	$[-0.3, 0.03]$	$[0.38, 1.79]$	$[1.66, 2.77]$	$[0.10, 0.27]$	$[0.066, 0.15]$	$[0.89, 2.96]$
RANS results [2]	-	-	[1.637,2.004]	-	$[0.134, 0.143]$	$[1.25, 2.84]$
Lyn *et al.*	-	-	2.1	-	0.132 ± 0.004	1.4

Table 4: Bulk coefficients; comparison with experimental data and with other simulations described in the literature.

4.6 Comparison with the experiments

The simulation that will be described here has been obtained on the computational domain (b). The parameters used for this simulation are the following:

γ_{scheme}	β	CFL max	C_s	Δ_{eq}
0.2	1/3	10	0.1	Def. (73)

The $CFL = 10$ for this grid corresponds to a non-dimensional time ($dt^* = dtU_\infty/D$) $dt^* = 0.008$. For each shedding cycle about 1000 time steps are employed.

The predicted bulk coefficients are reported in Tab. 4 together with the experimental data. In Refs. [2, 23] the results from several large-eddy and RANS simulations for this particular test-case are reported and compared. Thus, one could say that the solutions given in Refs. [2, 23] represents the state of the art of numerical simulation for the considered flow. In Tab. 4 we have reported the range of the bulk coefficients obtained in these simulations in order to give an idea of how our results compare with those in Refs. [2, 23]. Note that an unstructured grid has been employed here, while all the simulations in Refs. [2, 23] were performed on structured grids. This has allowed us to obtained a satisfactory refinement of the grid near the body with a low global number of nodes. In the simulations described in Ref [23], the number of nodes employed varies in the range [80000, 3800000], but a number of nodes lower than 110000 was used only in two simulations over 16.

The Strouhal number has been quite well predicted in our simulations, almost within experimental accuracy. The drag coefficient is underestimated if compared to the experimental one. The error committed is around 10%. The main causes for this error seem to be the following:

1. the insufficient distance between the inflow surface and the cylinder; indeed, from an analysis of the time-averaged pressure field we have seen that the influence of the cylinder propagates until the inflow boundary, and here it is still relevant;

2. the insufficient width of the computational domain. The slip conditions imposed on the side surface generates a situation of confined flow. This is put in evidence in Fig. 11,

where the time averaged velocity field in the rear area of the cylinder are plotted. It is possible to see that, due to the side surfaces, two counter rotating vortices are generated in the flow. This non physical three dimensional effects could explain the under estimation of the time-averaged drag coefficient with respect to the experiments. In order to try to check the qualitative effect of the side surfaces on the forces exerted on the body, we have estimated lift and drag curves using all the body nodes in one case and just the nodes located in the center of the cylinder (on a strip large $2D$) in the second case. We observed that, while the lift curves in the two different cases are almost identical, the drag curves are very different. Thus it seems that the side surfaces have strong influence on the drag.

In Fig. 12, 13, 14 the time averaged horizontal velocity field, plotted with a solid line, is compared with experiments [21]. As a general trend, the comparison with experiments is not satisfactory approaching to the body. A possible explanation could be the lack of resolution in those areas. This was also a general problem observed in the LES simulations presented in Ref. [23]. This problem could also be caused by the fact that we impose that the instantaneous velocity follows the Reichardt wall-law at the body. While this assumption seems to be plausible for time averaged velocities and has been found to give good results in RANS simulation, also in presence of separated regions, it is not clear if it is still valid in LES in which instantaneous velocities are computed at each time step. In Fig. 12 it is possible to note that the negative peak of velocity in the recirculation bubble behind the cylinder is overestimated by approximately a factor 2. The error in the prediction of the recirculating length is around 12%. It has been shown in [23] that this is a difficult quantity to be estimated from a simulation. Indeed, there are large differences among the different simulations and a very few of them gave a prediction of this length within an error of 5%. After the recirculation area, the simulation fits better with the experimental data until $X/D \simeq 4$. After this distance the results start to be influenced by the boundary conditions at the outflow, and this could explain the increasing difference from the experimental values we can observe for $x/D > 4$. This is also a common behavior of the LES simulations reported in Ref. [23]. The velocity u fits better with the experimental data in other areas out of the wake, as it is shown in Fig 13, 14.

In Fig. 15 we present the time averaged pressure coefficient obtained on the cylinder surface. The pressure coefficient is defined as follows:

$$C_p = \frac{2\,(p - p_\infty)}{\rho_\infty U_\infty^2}$$

where p_∞, rho_∞, U_∞^2 are respectively the pressure, the density and the velocity of the undisturbed flow, and p is the local pressure.

Experimental data for this parameter exist and they are reported in Ref. [1] for a Reynolds number of 50000. The pressure field on the front face of the cylinder is also well predicted. The shape of the pressure distribution on the rear face is well predicted, but the error on the numerical value of Cp with respect to the experimental data is about 7%. This explains the error committed in the prediction of the drag coefficient. There are

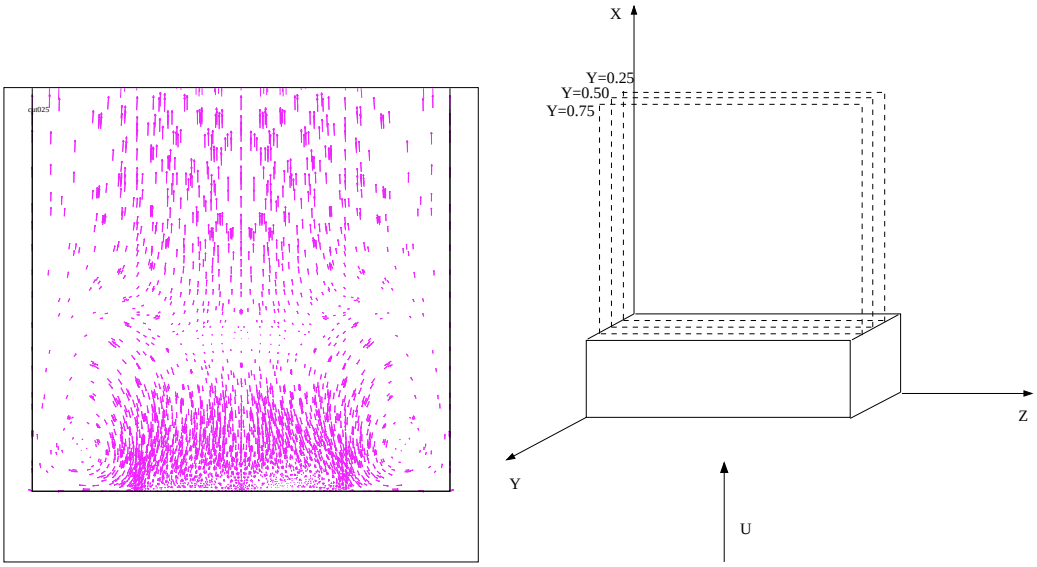

(a) Y/D=0.75

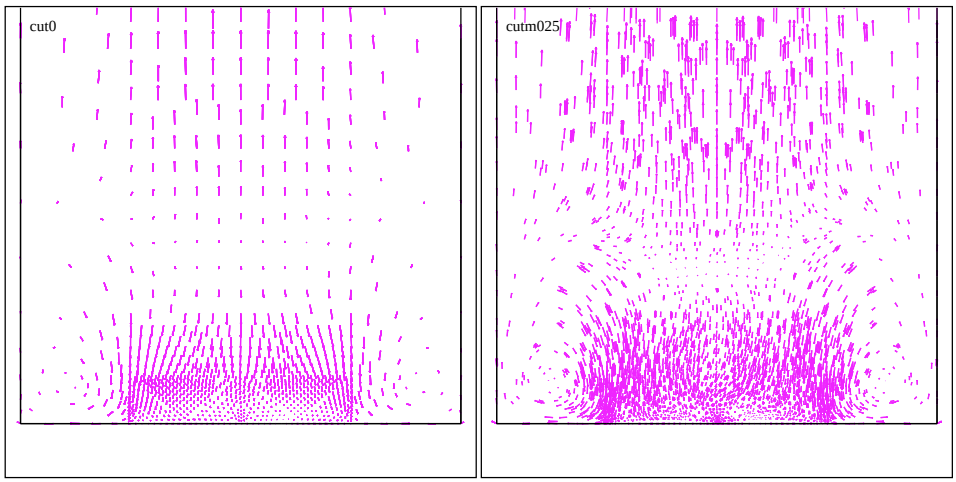

(c) Y/D=0.5 Y/D=0.25

Figure 11: Time averaged velocity field in the wake.

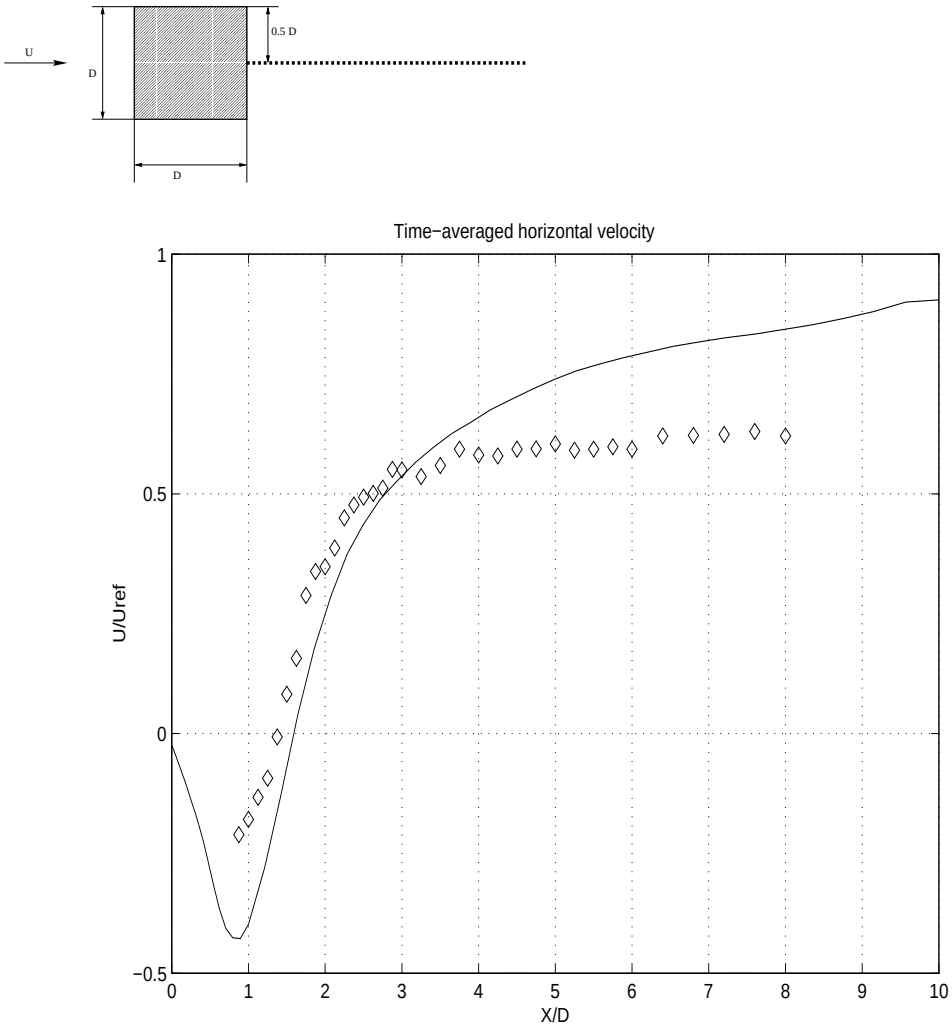

Figure 12: Mean horizontal velocity on the symmetry line of the cylinder.

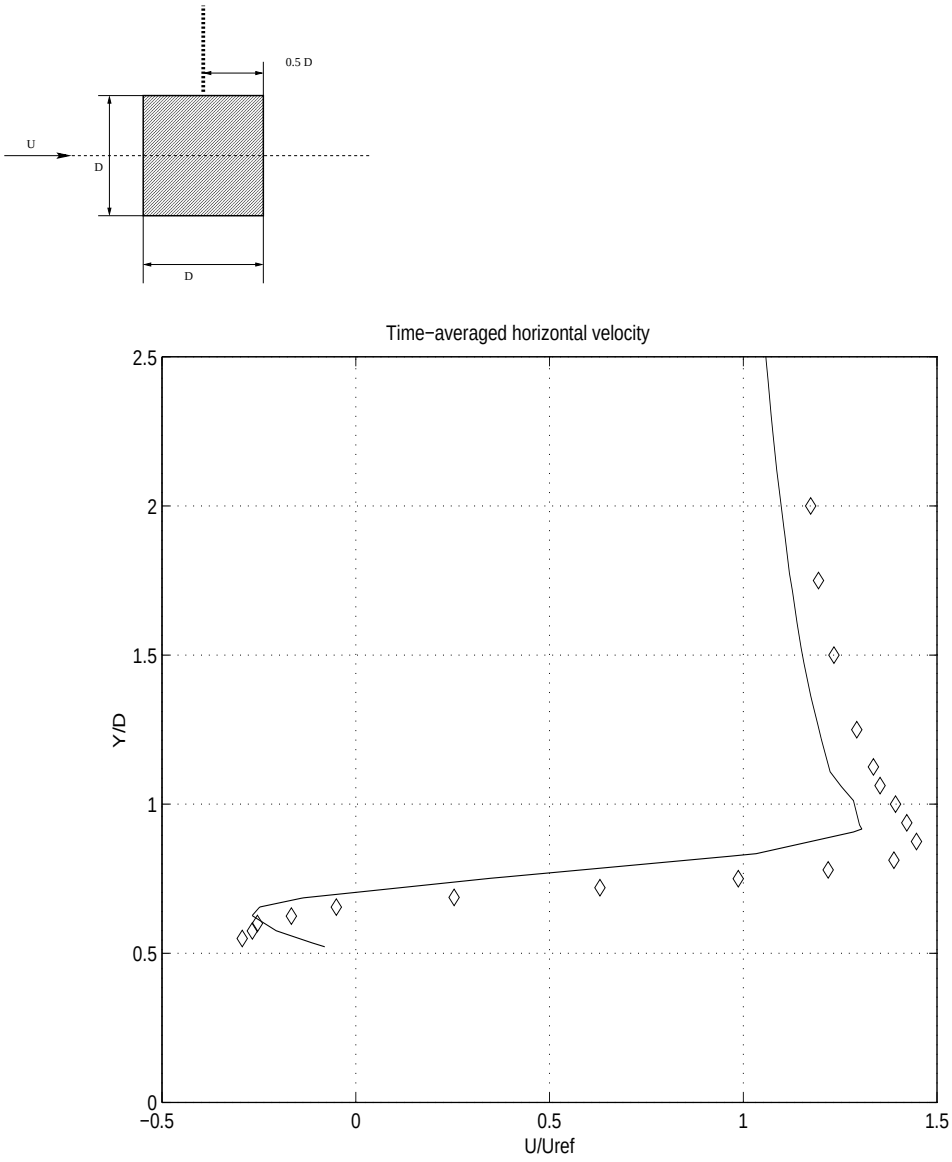

Figure 13: Mean horizontal velocity distribution (simmetry plane of the cylinder).

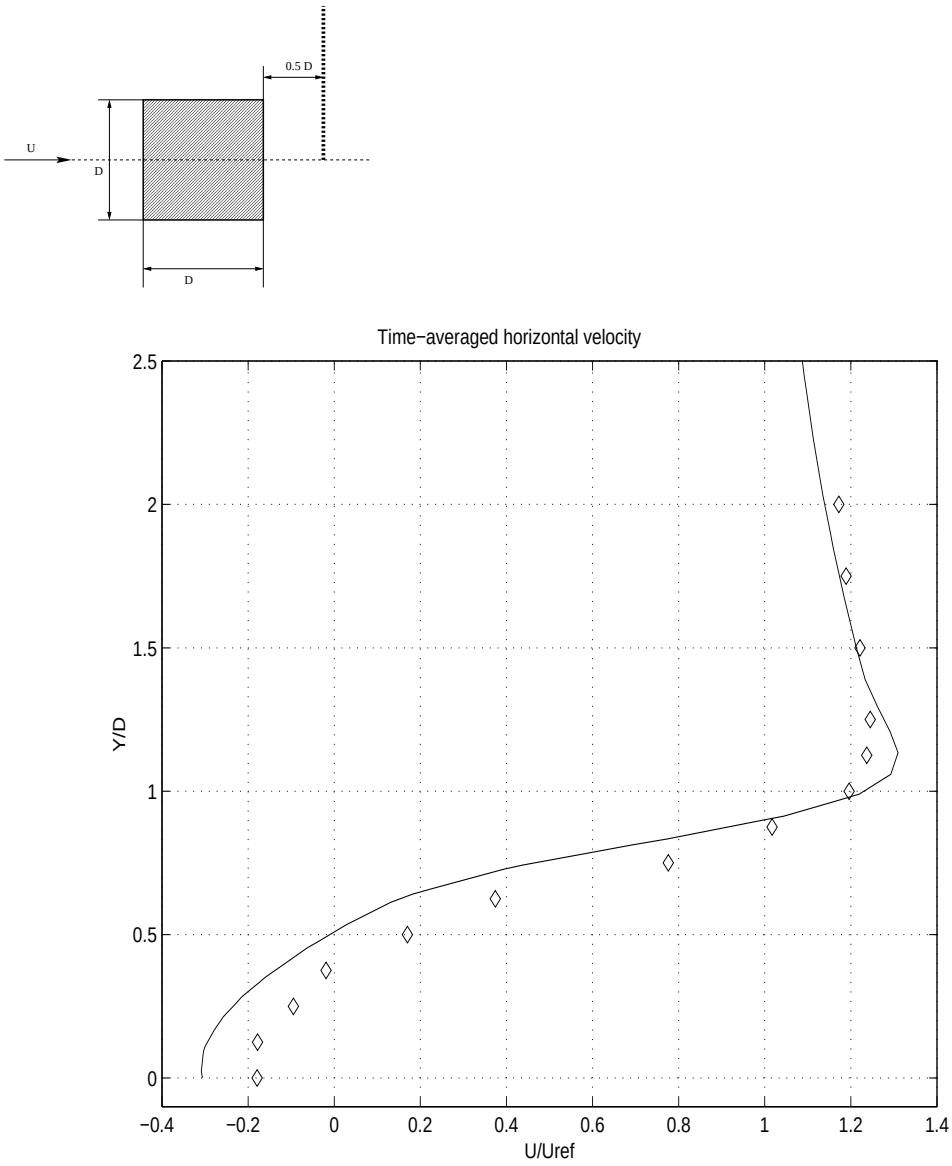

Figure 14: Mean horizontal velocity distribution (simmetry plane of the cylinder).

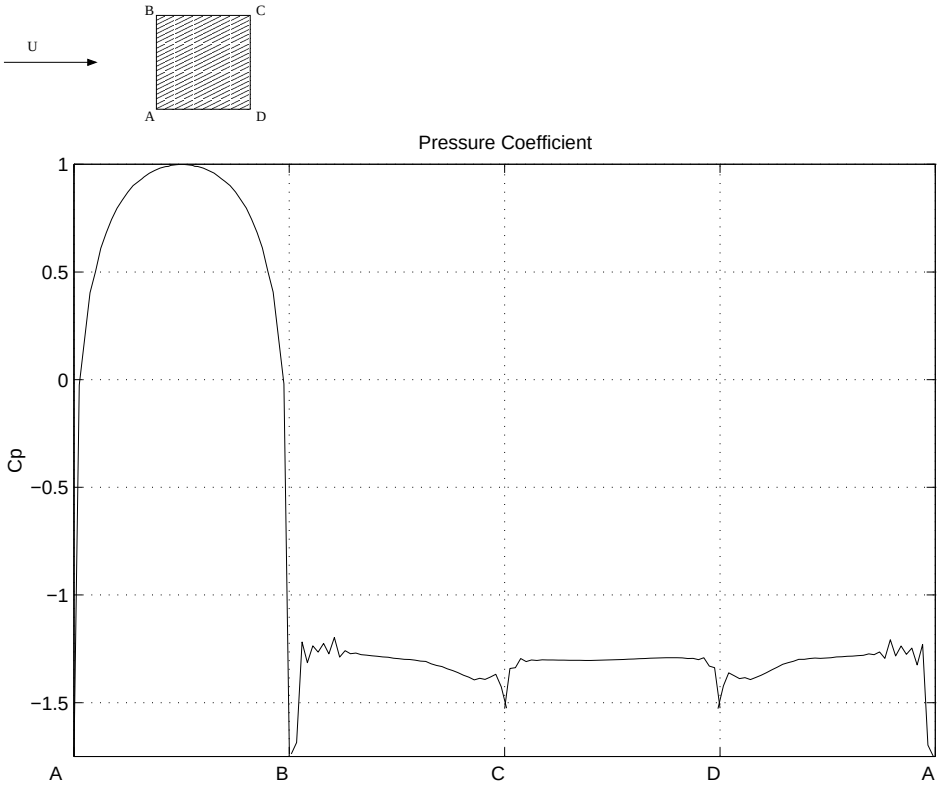

Figure 15: Pressure coefficient on the surface.

some problems in the prediction of the pressure coefficient on the upper and lower sides; since the flow is averaged in time, the two distribution are identical and this proofs that the averaging period employed was sufficiently long. The problems are connected to the front corners of the cylinder. Indeed, in this area we can observe an oscillatory behavior of the time averaged pressure. This problem could be related with a lack of resolution near the corner, that is a singular point for the flow. This could also be a consequence of the low values of numerical viscosity used for the simulation. Indeed, while the SGS viscosity acts as a stabilizing term for the velocities, there is no stabilization term for the pressure.

As a conclusion, the results obtained for this test case are not completely satisfactory. Anyway, they are acceptable under the light of the present state of art for LES on bluff bodies.

5 Conclusions

A large-eddy simulation approach has been implemented in an existing CFD code designed for industrial applications. The formulation for compressible flows of the Smagorinsky model [17], has been used for the closure of the equations. This represents the starting point towards the application of the large-eddy approach to the simulation of complex engineering flows. The flow around a square cylinder at a Reynolds number of 22000 has been chosen for a first validation of the present method. Although this flow does not contain all the complexity of the typical engineering problems, it is well suited for validation since both experimental data [20, 21] and numerical results from several RANS [2] and LES simulations [23] are available.

Since few applications of LES to real engineering flows can be found in the literature, many problems related to the use of LES within industrial codes still need to be investigated. In particular, the interaction between the numerical viscosity introduced by TVD schemes and the SGS viscosity has been investigated here. It has been shown that the numerical viscosity heavily interacts with the SGS model and it should be reduced as much as possible in order to obtain reliable results. However, a minimum amount of upwinding is necessary for the stabilization of the simulation. On the other hand, it has been shown that the SGS viscosity acts as a stabilizing term for the velocities and significantly less upwinding than without SGS models is necessary. In some numerical methods for the incompressible case, as it is the case of the MAC approximation or the Taylor-Hood mixed finite element method, the pressure is stabilized by the use of staggered grids. In the TVD schemes, the pressure, as well as the other flow parameters, is stabilized by the upwinding of the scheme. Since there are not SGS terms for the stabilization of the pressure, we risk to obtain an non-physical oscillatory behavior of the pressure field when the numerical viscosity is very low, as in the present simulations. This is in particular a problem for singularities, as, for instance, the cylinder corners in the considered test-case. At the same time, if a transonic or supersonic flow is simulated, the upwinding is necessary to stabilize the simulation near the shock waves. In this case, we should employ a shock detecting method in order to use the full upwinding only in localized areas around the flow singularities. Some simulations have been performed without any SGS viscosity; the results obtained were physically not consistent, and this proves that, at least for this test-case, the numerical viscosity cannot replace the SGS viscosity and that a SGS model is thus necessary. The ratio between the global approximation error, due to for the discretization of the equations, and the SGS viscosity effect has not been estimated here. This point needs to be investigated.

In industrial codes an implicit scheme for the time advancing is usually employed to increase the allowable time-step size. On the other hand, if the time step is too large, some significant time fluctuations of the resolved scale could be filtered out. If no additional modeling for time fluctuations is provided, this problem should be avoided by properly limiting the time step. The size of the maximum time step allowable is dependent on the coarseness of the mesh and on the kind of flow at issue. For the square cylinder test-case, a rule of thumb was used for the evaluation of the proper time advancing, and a $CFL = 10$ has been shown to be proper for the LES simulation. Thus, it has been shown here that the

use of an implicit scheme is still interesting for an LES approach, since the time step for the simulation can be considerably bigger that the maximum one we could use with an explicit scheme.

The implicit filter corresponding to the numerical scheme employed on unstructured grids is unknown a priori and very complex to determine. However, we need to define the equivalent filter width to obtain the SGS viscosity by the Smagorinsky model and this would require the knowledge of the applied filter. In this work we have studied in a-priori tests the behavior of two different definitions of the filter width as a function of the local shape of the grid. One of those definitions was already used in LES simulations on unstructured grids by Marquez [22]. It has been shown that their qualitative behavior is very similar and that they differ only quantitatively. Thus, with a proper choice of the Smagorinsky constant we should obtain the same results with the two different definitions. On the other hand, it has been shown that, for this particular test case, the sensitivity of the solutions to variations in the Smagorinsky constant are low. As a consequence, the two definitions of the filter width are somewhat equivalent. However, the correspondence between the numerical discretization on unstructured grids and the filter applied to the equations, is certainly a point worthwhile to be investigated in the future to obtain more reliable definitions of the filter width.

The results obtained in a simulation, in which the different input parameters were set on the basis of the sensitivity analysis previously described, have been compared in details with the experimental data and other numerical results. The agreement with experiments is not completely satisfactory, but our results are competitive with those obtained in the LES simulations reported in Ref. [23], in particular considering the fact that our grid is noticeably coarser.

Some discrepancies are observed in particular near the wake near the body. Note however that that is common to almost all the simulations in Ref. [23]. In our case this behavior could be explained by the lack of resolution in this region or by the use of a wall law. Indeed, in order to avoid the solution of the flow near the wall, which is computationally too expansive for engineering purposes, the Reichardt wall law has been employed. As stated in Sec. 2.7, this wall law gives an approximate description of the time-averaged near-wall velocity field. As a consequence, it is not clear whether LES can be coupled directly with the Reichardt wall-law, since the instantaneous velocity field is computed at each time-step, while, as said previously, a time-averaged tangential velocity is needed as an input for the wall law. The fact that the global results obtained in the simulation are not so far from the experimental one is an indirect proof that this coupling, also if conceptually not right, does not give completely wrong predictions. However, this point needs to be further investigated. At the same time, new approaches for the use of this wall-law for LES need to be proposed and validated.

Summarizing, the originality of this work is the combination of upwind stabilization, unstructured grid, implicit time advancing and the Reichardt wall law with the LES of compressible turbulence. All those elements are features dedicated to industrial abilities of the method. Numerical results are competitive for the considered test case with incompressibe

flow solvers that do not involve most of the above features. The use of very heterogeneous meshes and implicit time stepping is illustrated and it validates our proposition for affordable industrial LES.

Aknowledgements

The authors whish to thank A. Devieux for the important help given in the development of the present work. They also wish to thank all the Sinus team for the kind hospitality, the scientific support and the useful discussions.

The simulations reported here have been performed in Charle Hermite computer center in Nancy.

References

[1] P. W. Bearman and D. M. Trueman, 'An investigation of the flow around rectangular cylinders', *Aeronaut. Q.*, **23**, 1-6, (1971).

[2] G. Bosh and W. Rodi, 'Simulation of vortex shedding past a square cylinder with different turbulence models', *Int. J. Numer. Meth. Fluids*, **28**, 601-616, (1998).

[3] F. H. Champagne, C. A. Friehe, J. C. La Rue and J. C. Wyngaard, 'Flux measurement, flux estimation techniques and fine-scale turbulence measurements in the unstable surface layer over land', *J. Atmos. Sci.*, **34**, 515-530, (1977).

[4] R. Carpentier, 'Comparison entre des schémas 2D de type Roe sur maillage régulier triangle ou quadrangle', *INRIA REPORT 3360*, (1998).

[5] J.W. Deardorff, 'A numerical study of three-dimensional turbulent channel flow at large Reynolds numbers', *J. Fluid Mech.*, **41**, 453-480, (1970).

[6] D. F. G. Durao, M. V. Heitor, J. C. F. Pereira, 'Measurements of turbulent and periodic flows around a square cross-section cylinder', *Exp. Fluids*, **6**, 298-304, (1984).

[7] G. Erlebacher, M.Y. Hussaini, C.G. Speziale, T.A. Zang, 'Toward the large-eddy simulation of compressible turbulent flows', *J. Fluid Mech.*, **238**, 155-185, (1992).

[8] C. Farhat, B. Koobus, H. Tran, 'Simulation of Vortex Shedding Dominated Flows Past Rigid and Flexible Structures', *Computational Methods for Fluid-Structure Interaction*, ed. T. Kvamsdal, I. Enevoldsen, K. Herfjord, C. B. Jenssen, K. Mehr and S. Norsett, Tapir, 1-30, (1999).

[9] A. Favre, 'Turbulence: space-time statistical properties and behavior in supersonic flows', *Phys. Fluids*, **26**, 2851-2863, (1983).

[10] J. Francescatto, 'Méthodes multigrilles par agglomération directionnelle pour le calcul d'écoulements turbulents', *Thèse Université de Nice-Sophia Antipolis*, (1998).

[11] E. Garnier, P. Sagaut, P. Comte, M. Deville, 'On the Use of Shock-Capturing Schemes for Large-Eddy Simulation', *J. Comp. Phys.*, **153**, 273-311, (1999).

[12] M. Germano, U. Piromelli, P. Moin, W. Cabot, 'A dynamic subgrid-scale eddy viscosity model', *Phys. Fluids*, **A3(7)**, 1760-1765, (1991).

[13] J.O. Hinze, *Turbulence*, McGraw-Hill, New York, (1959).

[14] K. Jansen, 'Unstructured grid large eddy simulation of flow over an aerfoil', *Annual Research Briefs 1994*, Center for Turbulence Research, NASA Ames/Stanford Univ., 161-174, (1994).

[15] K. Jansen, 'Preliminary large-eddy simulations of flow around a NACA 4412 aerfoil', *Annual Research Briefs 1995*, Center for Turbulence Research, NASA Ames/Stanford Univ., 61-72, (1995).

[16] B. E. Lee, 'The effect of turbulence on the surface pressure field of a square cylinder', *J. Fluid Mech.*, **69**, 263-282, (1975).

[17] M. Lesieur, P. Comte, 'Turbulence in compressible flows', *AGARD-R-819*, 4.1-4.39, (1997).

[18] M. Lesieur, O. Métais, 'New trends in Large-eddy simulations of turbulence', *Annu. Rev. Fluid Mech.*, **28**, 45-82, (1996).

[19] D.K. Lilly, 'The representation of small-scale turbulence in numerical simulation experiments', *Proceedings of IBM Scientific Computing Symposium on Enviromental Science*, IBM form N.**3**20-1951, 1967.

[20] D. A. Lyn, W. Rodi, 'The flapping shear layer formed by flow separation from the forward corner of a square cylinder', *J. Fluid Mech.*, **267**, 353-376, (1993).

[21] D. A. Lyn, S. Einav, W. Rodi, J. H. Park, 'A laser-Doppler velocimeter study of ensemble-averaged characteristics of the turbulent near wake of a square cylinder', *J. Fluid Mech.*, **304**, 285-319, (1995).

[22] B. Marquez, 'Simulation des grandes echelles d'encoulements compressible par des méthodes eléments finis', *Thèse Université de Toulouse*, (1999).

[23] W. Rodi, J. H. Ferziger, M. Breuer, M. Pourquié, 'Status of Large Eddy Simulation: Results of a Workshop', *Transactions of ASME*, **119**, 248-262, (1997).

[24] P.L. Roe, 'Approximate Riemann Solvers, Parameters, Vectors and Difference Schemes', *J. Comp. Phys.*, **43**, 357-372, (1981).

[25] J. Smagorinsky, 'General circulation experiments with the primitive equations', *Mon. Weather Rev.*, **91(3)**, 99-164, (1963).

[26] J.L. Steger, R.F. Warming, 'Flux Vector splitting for the inviscid gas dynamic equations with applications to finite difference methods', *J. Comp. Phys.*, **40**, 263-293, (1981).

[27] B. Van Leer, 'Flux Vector Splitting for the Euler equations', *Lecture notes in Physics*, , 170, (1982).

[28] O. V. Vasilyev, T. S. Lund, 'A general theory of discrete filtering for LES in complex geometry', *Annual Research Briefs 1997*, Center for Turbulence Research, NASA Ames/Stanford Univ., 67-82, (1997).

[29] B. Vreman, B. Geurts, H. Kuerten, 'A priori tests of large eddy simulation of the compressible plane mixing layer', *J. Fluid Mech.*, **29**, 299-327, (1995).

[30] A. Yoshizawa, 'Subgrid-scale modeling of compressible turbulent flows', *Phys. Fluids*, **A3(4)**, 714-716, (1991).

Unité de recherche INRIA Sophia Antipolis
2004, route des Lucioles - B.P. 93 - 06902 Sophia Antipolis Cedex (France)

Unité de recherche INRIA Lorraine : Technopôle de Nancy-Brabois - Campus scientifique
615, rue du Jardin Botanique - B.P. 101 - 54602 Villers lès Nancy Cedex (France)
Unité de recherche INRIA Rennes : IRISA, Campus universitaire de Beaulieu - 35042 Rennes Cedex (France)
Unité de recherche INRIA Rhône-Alpes : 655, avenue de l'Europe - 38330 Montbonnot St Martin (France)
Unité de recherche INRIA Rocquencourt : Domaine de Voluceau - Rocquencourt - B.P. 105 - 78153 Le Chesnay Cedex (France)

Éditeur
INRIA - Domaine de Voluceau - Rocquencourt, B.P. 105 - 78153 Le Chesnay Cedex (France)
http://www.inria.fr
ISSN 0249-6399